Carbon Materials Prepared *via* Green Hydrothermal Carbonization of Water Hyacinth (*Eichhornia crassipes*)

Amonrada Saning

A Thesis Submitted in Partial Fulfillment of the Requirements for the Degree of Master of Science in Chemistry

Prince of Songkla University

2019

Carbon Materials Prepared *via* Green Hydrothermal Carbonization of Water Hyacinth (*Eichhornia crassipes*)

Amonrada Saning

A Thesis Submitted in Partial Fulfillment of the Requirements for the Degree of Master of Science in Chemistry

Prince of Songkla University

2019

Thesis Title	Carbon Materials Prepared *via* Green Hydrothermal Carbonization of Water hyacinth (*Eichhornia crassipes*)
Author	Miss Amonrada Saning
Major Program	Chemistry

Major Advisor

.....

(Dr.Laemthong Chuenchom)

Co-advisor

.....

(Assoc. Prof. Dr.Pongsaton Amornpitoksuk)

Examining Committee:

.....Chairperson

(Dr.Decha Dechtrirat)

.....Committee

(Assoc. Prof. Dr.Pongsaton Amornpitoksuk)

.....Committee

(Asst.Prof.Dr.Uraiwan Sirimahachai)

.....Committee

(Dr.Laemthong Chuenchom)

The Graduate School, Prince of Songkla University, has approved this thesis as Partial fulfillment of the requirements for the Master of science Degree in Chemistry

.....

(Prof.Dr. Damrongsak Faroongsarng)

Dean of Graduate School

This is to certify that the work here submitted is the result of the candidate's own investigations. Due acknowledgement has been made of any assistance received.

.....Signature
(Dr.Laemthong Chuenchom)
Major Advisor

.....Signature
(Assoc.Prof.Dr.Pongsaton Amornpitoksuk)
Co-advisor

.....Signature
(Miss Amonrada Saning)
Candidate

I hereby certify that this work has not been accepted in substance for any degree and is not being currently submitted in candidature for any degree.

.....Signature
(Miss Amonrada Saning)
Candidate

ชื่อวิทยานิพนธ์ วัสดุคาร์บอนที่เตรียมโดยผักตบชวาผ่านกระบวนการไฮโดรเทอร์มัลคาร์บอไนเซชั่น

ผู้เขียน นางสาวอมลรดา สานิง

สาขาวิชา เคมีเชิงฟิสิกส์

ปีการศึกษา 2561

บทคัดย่อ

ผักตบชวา (*Eichhornia crassipes*) เป็นวัชพืชต่างถิ่นได้ถูกเปลี่ยนให้เป็นวัสดุคาร์บอนผ่านกระบวนการไฮโดรเทอร์มัลคาร์บอไนเซชั่นซึ่งเป็นกระบวนการที่ให้พลังงานต่ำและเป็นมิตรต่อสิ่งแวดล้อม โดยกระบวนการดังกล่าวให้ผลิตภัณฑ์ออกมาทั้งในรูปของแข็งและของเหลว ผลิตภัณฑ์ในส่วนของแข็งหรือไฮโดรชาร์ถูกเพิ่มคุณสมบัติแม่เหล็กโดยการเติม Fe^{3+} และกระตุ้นทางเคมีเพื่อเพิ่มรูพรุนให้กับวัสดุโดยใช้ KOH วัสดุคาร์บอนที่ได้มีคุณสมบัติแม่เหล็กที่ดีและถูกนำไปใช้เป็นตัวดูดซับในการกำจัดสีย้อม (เมทิลีนบลูและเมทิลออเรนจ์) และเตตราไซคลิน โดยให้ค่าการดูดซับสูงถึง 524.20 (เมทิลีนบลู), 425.15 (เมทิลออเรนจ์) และ 294.24 mg g^{-1} (เตตราไซคลิน) ซึ่งเป็นผลมาจากพื้นที่ผิวที่สูงและมีรูพรุนขนาดกลางซึ่งช่วยในการดูดซับสารโมเลกุลขนาดใหญ่ นอกจากนี้ผลิตภัณฑ์ในส่วนของเหลวซึ่งสามารถละลายน้ำได้ดี ถูกนำไปกระตุ้นด้วย KOH ในอัตราส่วนที่ต่ำเพื่อเพิ่มพื้นที่ผิวให้กับวัสดุ โดยวัสดุที่เตรียมได้มีพื้นที่ผิวสูงถึง 2,545 cm^2 g^{-1} ซึ่งเหมาะสมกับการนำไปใช้เป็นตัวเก็บประจุยิ่งยวด เมื่อศึกษาประสิทธิภาพของตัวเก็บประจุที่เตรียมได้พบว่ามีค่าการเก็บประจุจำเพาะ อยู่ที่ 100 F g^{-1} ที่ 1 A g^{-1} และยังคงมีประสิทธิภาพการเก็บประจุสูงถึง 92% แม้ผ่านการใช้งานมาแล้วกว่า 10,000 รอบ ในงานวิจัยชิ้นนี้แสดงให้เห็นว่ากระบวนการไฮโดรเทอร์มัลคาร์บอไนเซชั่นเป็นกระบวนการที่มีประสิทธิภาพในการเปลี่ยนชีวมวลให้เป็นวัสดุคาร์บอนที่มีคุณค่า สามารถใช้ประโยชน์ได้ทั้งผลิตภัณฑ์ในส่วนของแข็งและของเหลว

Thesis Title Carbon materials prepared *via* green hydrothermal carbonization of water hyacinth (*Eichhornia crassipes*)

Author Miss Amonrada Saning

Major program Physical Chemistry

Academic Year 2018

Abstract

Troublesome aquatic weed, water hyacinth (*Eichhornia crassipes*) was converted into solid and liquid fractions *via* green and energy-saving hydrothermal carbonization (HTC). The solid product, hydrochar, was employed as a precursor to prepare magnetic carbon materials by simple activation and magnetization using KOH and Fe^{3+} ions, respectively. The obtained magnetic adsorbent possessed good magnetic properties and presented outstanding capacities to adsorb methylene blue (524.20 mg g^{-1}), methyl orange (425.15 mg g^{-1}) and tetracycline (294.24 mg g^{-1}) with rapid adsorption kinetics even at high concentrations (up to 500 mg L^{-1}), attributed to high specific surface area and mesopore porosity. Besides the solid hydrochar, the water-soluble liquid product was used to fabricate carbon-based supercapacitors through facile KOH activation with considerably lower KOH amount in comparison to conventional activation. The supercapacitor electrode made from activated liquid product possessed an extremely high specific surface area of 2545 cm^2 g^{-1} and showed excellent specific capacitance (100 F g^{-1} or 50 F cm^{-3} at 1 A g^{-1}) and good retention of capacitance (92% even after 10,000 cycles). This work demonstrated that both solid and liquid HTC fractions from this bio-waste can serve as effective sources to prepare functional carbon materials, making this approach a sustainable zero-waste biomass conversion process.

ACKNOWLEDGEMENTS

I would like to sincerely thank to Dr. Laemthong Cheunchom, my advisor, for useful suggestion, criticism, encouragement and especially unbroken patience during my research experiment period and this thesis improvement.

I would like to express my special thanks to Assoc. Prof. Dr. Pongsaton Amornpitoksuk, my co-advisor, and Asst. Prof. Dr. Uraiwan Sirimahachai who contributed their time for reviewing and improving this thesis.

I am grateful to Dr. Decha Dechtrirat, the examining chairperson for fruitful suggestion and correction of this thesis

I would like to thank Dr. Servann Herou, post-doctoral researcher from Imperial College London, London, UK for accomplishing and suggesting the electrochemical study

I would like to thank Department of Chemistry, Faculty of Science, Prince of Songkla University for equipment support.

I would like to thank Science Achievement Scholarship of Thailand (SAST), Center of Excellence for Innovation in Chemistry (PERCH-CIC) and Newton Fund – Thailand Research Fund Institutional Links 2018/19 program (grant no. RDG62W0001) for financial support.

Finally, I would like to genuinely thank my family and my friends who always support and encourage me in the hardest time.

Amonrada Saning

THE RELEVANCE OF THE RESEARCH WORK TO THAILAND

Water hyacinth (*Eichhornia crassipes*) is a floating aquatic weed. It is considered as the invasive species which severely spreads around the world including Thailand. Due to its uncontrollable growth, it blocks the water surface and impedes the water body from oxygen and sunlight which eventually cause water pollution and thereby ruining the ecosystem. However, there is not many effective methods reported about this problem solving.

In this research, the valorization of water hyacinth into value-added carbon materials (magnetic carbon adsorbent and supercapacitor) *via* a green hydrothermal carbonization was demonstrated in order to purpose the potential usage of this invasive alien species. The results from this thesis could lead to the transfer of knowledge into the practical applications.

CONTENT

Page

LIST OF FIGURES

Figure **Page**

LIST OF TABLES

Table **Page**

CHAPTER 1

INTRODUCTION

1.1 Introduction

Water hyacinth (WH, *Eichhornia crassipes*) is a floating aquatic weed originating from South America. It is considered an invasive species that has spread around the world. In many countries, including Thailand, Indonesia, and China, WH reproduces very quickly, covering large water bodies including rivers, lakes and canals, impeding water flow, and starving the water of oxygen. This often kills fish and other species and reduces biodiversity[2]. It has been reported that it takes only one day to reproduce over one-fourth tons of dried WH per hectare[2]. Nowadays, attempts at beneficial utilization of WH have been spent mostly on handicraft products[3] and fertilizers[4]. However, regarding the economic merits of this approach, such products do not provide much value. The real problem is that WH grows at a rate that surpasses its consumption. Therefore, to address this problem in an economically viable fashion, the WH needs new innovative uses.

Considering its chemical composition, WH has notable lignocellulosic content, including 48% hemicellulose as the major component, along with 20% cellulose and 3.5% lignin[4]. Since WH has excessive reproduction rate and is rich in cellulose, hemicellulose and lignin, it can potentially be employed as a proper carbon source. For this reason, considerable attention has been paid to the use of WH to prepare functional carbon materials or value-added chemicals[3], [5]–[11].

Hydrothermal carbonization (HTC) is a simple process to convert biomass into carbon materials, performed using water as the medium in a closed system at self-generated pressure and moderate temperatures (150-350 °C)[12], [13]. The process involves hydrolysis and dehydration of lignocellulosic compounds in the biomass. Unlike conventional pyrolysis at higher temperatures, a prominent reason making HTC an attractive method is that the outcome products are in both solid and liquid forms, and the treatment temperatures are relatively low. The solid product from HTC is hydrochar with surfaces that are rich in oxygenated functional groups[13], [14]. The abundant oxygen in these groups provides hydrophilicity to the hydrochars, and facilitates use as catalysts, or as adsorbents of polar or cationic guest molecules[14]–

[16]. However, hydrochar typically has poor porosity that reduces its suitability for adsorbent, which needs to have large specific surface for adsorption capacity. Aside from the solid hydrochar, the liquid product from HTC contains various valuable platform chemicals soluble in water, for example levulinic acid, hydroxymethylfurfural (HMF), furfural, phenolic compounds, and lignin compounds[17]. Although these compounds are attractive as biofuels, fractionating them would be time- and energy-consuming, and require the use of expensive catalysts to convert the fractions to higher value chemicals[18]–[20].

Only a few studies have reported on direct uses of this liquid product from HTC for the synthesis of solid carbon materials[21], [22]. Bai and co-workers[22] used black liquor, the liquid product from KOH-assisted HTC of rice straw, to prepare a carbon-based acid catalyst. The study suggested that the liquid product has promising potential as carbon source in carbon material synthesis. Shortly after, Zhu et al.[21] prepared N-doped supercapacitors using the liquid product or black liquor from HTC of rice straw in the presence of KOH. It is clear that the high water-solubility of black liquor has enabled an alternative way to ensure homogeneous integration of other elements or compounds into the final carbon materials.

To the best of our knowledge, only a few publications have mentioned the use of both phases from HTC to fabricate functional materials for different applications.[23] In this current study both solid hydrochar and liquid fractions from HTC of WH are used as precursors to prepare magnetic adsorbents and a supercapacitor, respectively. The magnetic adsorbents have superior adsorption of toxic chemicals (dyes and tetracycline) and the supercapacitor has excellent specific capacitance and good capacitance retention. It is also worth mentioning that our proposed methods mainly employed water as the medium in all steps, totally excluding toxic organic solvents, thereby making the processes environmentally friendly.

This study demonstrates that undesired WH biomass can be easily transformed into functional carbon materials with multiple uses, by using both the solid and the liquid fractions from HTC. This concept of converting WH biomass into high value-added functional materials appears sustainable and does not generate waste.

1.2 Preliminary knowledge and Theoretical section

1.2.1 Hydrothermal carbonization

Hydrothermal carbonization is a process converting carbon precursor into carbon materials using low temperature. The experiment is performed in closed system and incorporates with water. During the process, the pressure is self-generated within the reactor and changes the water properties into an active form. In the initial period of HTC of biomass, the hydrolysis reaction takes the important role in converting cellulose in biomass into (oligo-) saccharides and dissolves the lignin fraction into the water phase which further was hydrolyzed into phenol compounds. Next, the hydroxyl groups were destroyed *via* the dehydration reaction which relates to the elimination of water from the precursor and the carboxyl functional group destruction was also conducted by decarboxylation step. Then the aromatization is taking place for conversion of double-bonded compounds into single bond groups. Furthermore, the final reaction involved in HTC process is re-condensation which mainly relate to the lignin fraction and lead to the formation of hydrochar.[16], [24]

1.2.2 Adsorption

Adsorption is the process happening on the surface of the materials. The phenomenon starts when the adhesion energy between solid materials surface (the adsorbent) and the adsorbate in gas or liquid phase becomes higher that the cohesion energy. The higher material surface area, the greater adsorption efficiency the materials provide. The fundamental mechanisms of the adsorption are physisorption and chemisorption. The physisorption or physical adsorption occurs when the adsorbent and adsorbate molecules are interacted using London-Van der Waal force. Another adsorption mechanism is chemisorption which relates to the chemical bonding of adsorbent and adsorbates.[25] This technique is widely used in industry section for wastewater remediation.

1.2.2.1 Adsorption kinetic

Adsorption kinetic is the experiment performing with certain amount of adsorbate and adsorbent in various time in order to study the effect of contact time on the adsorption behavior. This experiment provides the adsorption equilibrium time and adsorption rate calculating by adsorption kinetic models such as pseudo first- and pseudo second kinetic model[26].

(1) Pseudo first kinetic model

Pseudo first order kinetic model is one of the basic kinetic models purposed in 1898 by Lagergren. The model equation can be expressed in non-linear form as

$$q_t = q_e(1 - e^{-k_1 t}) \quad (1)$$

Where q_t and q_e are the adsorption capacity at certain time and at equilibrium, respectively. k_1 is the rate constant of pseudo first kinetic model[27].

(2) Pseudo second kinetic model

Pseudo second order is one of the most used kinetic models developed by Ho.[28] The pseudo second kinetic graph was presented by plotting adsorption capacity (q_t) versus the contact time. Furthermore, the adsorption rate could be expressed as

$$\frac{dq_t}{dt} = k_2(q_e - q_t)^2 \quad (2)$$

Where k_2 represents the pseudo second order fitted adsorption rate constant. Then the equation (1) was integrated using t=0 to t=t and q_t=0 to q_t = t as a boundary condition. The result is given as:

$$q_t = \frac{{q_e}^2 k_2 t}{1+q_e k_2 t} \quad (3)$$

1.2.2.2 Adsorption isotherm

Adsorption isotherm is the experiment studying the equilibrium state of the adsorption. The experiment could simply perform by mixing the certain amount of adsorbent with various concentration of adsorbate until the adsorption equilibrium has reached. The isotherm is plotted using the adsorption capacity at the equilibrium versus the equilibrium concentration[29].

(1) Langmuir isotherm

Langmuir isotherm, which originally purposed by Irving Langmuir, describes the behavior between homogeneous adsorbent surface and adsorbate molecules. The model assumes that there is monolayer adsorption on the surface of the adsorbent. The Langmuir model can be fitted using non-linear equation (3)

$$q = \frac{q_{max} K_L C_e}{1+K_L C_e} \quad (4)$$

Here q_{max} is maximum adsorption capacity, K_L is Langmuir constant and C_e is the equilibrium concentration[29].

(2) Freundlich isotherm

Unlike the Langmuir model, Freundlich model assumes that the surface of the adsorbent is heterogeneous and the adsorption between adsorbent and adsorbate molecules is formed in multilayer form[30]. The Freundlich model equation could be expressed as

$$q_e = K_F \cdot C_e^{1/nF} \quad (5)$$

Where K_F is Freundlich constant and n represents the empirical constant.

1.2.3 Supercapacitor

Supercapacitor is the alternative energy storage device. Despite the relatively low energy density compared to batteries, its high specific capacitance, favorable power density and great cyclability. the energy density and power density capability of supercapacitor could be illustrated using Ragone plot in figure 1

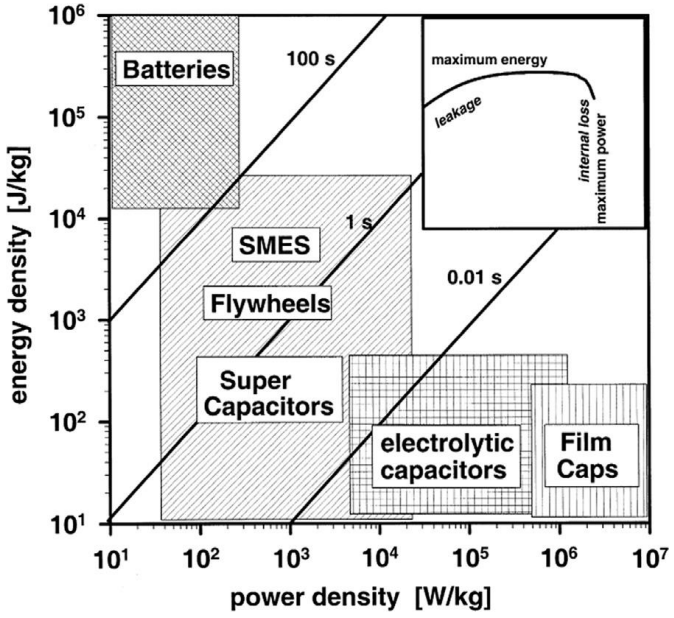

Figure 1 Ragone plot described energy and power density behavior of energy storage devices

There are 3 types of supercapacitors which are pseudocapacitors, electrochemical double-layer capacitors (EDLCs) and Hybrid capacitors defined by the interaction on the electrode surface. EDLCs relates to the adsorption and desorption of ion in the pores of the materials, especially micropores, the during charge/discharge processes. The capacitance of EDLCs depends on the thickness of the double layer of electrode and electrolyte. The pseudocapacitor relates to the faradaic reaction or redox reaction. This reversible oxidation and reduction process could enhance the capacitive performance of the preusocapacitor to over 10-100 times of EDLCs' capacitance. However, the drawbacks of this type of capacitor are the low cyclability due to the loss of functional group during faradaic process and its materials' low conductivity. The last type of capacitor is hybrid capacitor which is the combination between carbon and Li-ion electrode[31]–[33].

1.2.3.1 Carbon materials using as the supercapacitor electrode

Since carbon materials provide high surface area which enhances the performance of the electrode, carbon material is the most extensively chosen materials for supercapacitor electrode preparation, especially, activated carbon which is low cost and has an appropriate surface area[34].

1.2.3.2 Metal oxide using as the supercapacitor electrode

Metal oxide is one of the most effective materials using as supercapacitor electrodes. The factors making these materials a satisfactory precursor are its high conductivity and favorable specific capacitance. The most reported metal oxide-based supercapacitors are Ruthenium oxide and Manganese oxide[31].

1.3 Review of literature

In this thesis, the literature review is divided into 3 section which are 1) The biomass conversion using hydrothermal carbonization process 2) The preparation of magnetic carbon materials and 3) the fabrication of carbon-based supercapacitor

1.3.1 The biomass conversion using hydrothermal carbonization process

Ghadikolaei and coworkers (2019)[35] prepared the N-functionalized hydrochar through the hydrothermal carbonization of Tetra Amino Hyperbranched Polymer (TAHP) and walnut shell at 250 °C for 60 minutes. The optimized functionalized hydrochar has high surface area of 544 m^2 g^{-1}. The materials were further used as

adsorbents for Cr(VI) removal. The adsorption result shows that the optimized material provided highest adsorption efficiency of 363.22 mg g^{-1} according to Freundlich isotherm and kinetic result was fitted with pseudo-second-order kinetic model.

Li and coworker (2018)[36] prepared the adsorbent from bamboo sawdust using hydrothermal carbonization process in acid solution and two-stage hydrothermal carbonization. Then the obtain materials were used to study their adsorption efficiency on Congo red and 2- naphthol removal. The adsorption result demonstrated that the highest adsorption capacity provided by the selected adsorbents is 90.51 and 72.93 mg g^{-1} for Congo red and 2- naphthol, respectively.

Bai and coworkers (2016)[22] studied the fabrication solid acid catalyst from black liquor. The black liquor was obtained from liquid product of KOH-assisted hydrothermal carbonization at 120 °C for 4 hours. Then the obtained black liquor was further carbonized at 600 °C for 2 hours and heated in H_2SO_4 at 150 °C for 10 h to functionalize $–SO_3H$ groups. The final product was used as an effective catalyst for total reducing sugar production.

Zhu and coworkers (2017)[21] prepared the N-doped high-performance supercapacitor from saw dust derived black liquor from hydrothermal carbonization. First, saw dust was mixed with KOH solution and heated at 120 °C for 4 hours in Teflon lined stain-less steel autoclave. The liquid product was called black liquor. Afterwards, melamine was added into the black liquor as a nitrogen source and carbonized under N_2 atmosphere at 700-900 °C. The electrochemical experiment was performed with the optimized sample (carbonized temperature of 800 °C) and found that the specific capacitance of the materials is 337 F g^{-1} at current density of 0.5 A g^{-1} using 6 M KOH as electrolyte which demonstrated the high potential of using the materials as a supercapacitor.

All literatures suggest that hydrothermal carbonization is the appreciable method for biomass conversion into value-added materials since both liquid and solid product could be used as carbon precursor.

1.3.2 The preparation of magnetic carbon materials

Ifthikar and coworkers (2017)[37] fabricated the magnetic carbon adsorbent *via* the pyrolysis of sewage sludge and further activation using $ZnCl_2$. Afterwards, the magnetic property was added into the materials by precipitation of $FeCl_3{\cdot}6H_2O$ and

$FeSO_4 \cdot 7H_2O$ under basic solution. The obtained material was investigated its Pb(II) adsorption and found that the maximum adsorption capacity of the material is 249.00 mg g^{-1}.

Astuti and coworkers (2019)[38] prepared magnetic activated carbon from pineapple crown leaf. Activated carbon was prepared by carbonizing pineapple crown leaf at 500 °C for 90 minutes and KOH-activation using microwave oven. Then the obtained activated carbon was stirred in solution of $FeCl_3 \cdot 6H_2O$ and $FeSO_4 \cdot 7H_2O$ and NaOH solution was further added dropwise into the mixture in order to introduce the magnetic property. The result shows that the obtained materials have desirable surface area and pore texture suitable for dye removal. Moreover, the KOH also has an important role in porosity development.

Han and coworkers (2016)[39] prepared the magnetic biochar from peanut hull. First, ground peanut hull was stirred in $FeCl_3 \cdot 6H_2O$ solution, dried and carbonized under N_2 atmosphere at 450-650 °C for 1 hours. The XRD pattern showed that the iron species in the materials is γ-Fe_2O_3 which demonstrated good magnetization property. Furthermore, the materials were used as adsorbents for Cr(VI) removal.

The studies show that the addition of magnetism into the materials can be simply fabricated using co-precipitation of Fe(II)/Fe(III) in basic solution or carbonization Fe(III) at high temperature. In this work, $FeCl_3 \cdot 6H_2O$ and KOH were used as an iron source and activating agent, respectively.

1.3.3 The fabrication of carbon-based supercapacitor

An and coworkers (2017)[40] studied the preparation of supercapacitor from Agaric through KOH activation (precursor: KOH = 1:1) at 750 °C for 2 hours. The obtained material has high specific surface area 1565.6 m^2 g^{-1}. In term of electrochemical performance, the material exhibits outstanding specific capacitance of 324 F g^{-1} at a current density of 1 A g^{-1} in 1 M H_2SO_4 solution and good energy density of 27.2 Wh kg^{-1}.

Song and coworkers (2019)[41] successfully synthesized EDLCs from tea waste. The KOH activation process (precursor: KOH = 1:2) at 900 °C for 1 hours was performed to enhance the porosity of the materials. The result shows that the high surface material (911.92 m^2 g^{-1}) has excellent capacitive performance in term of cyclability (96.7 % capacitance retention after 16,000 cycles) and power density (3,494.70 W kg^{-1} at energy density of 19.45 Wh kg^{-1}).

Elaiyappillai and coworkers (2019)[42] prepared the supercapacitor from *Cucumis melo* peel through carbonization at 300 °C for 4 hours and further KOH activation at 600-900 °C for 3 hours. The outstanding specific capacitance of the material (404 F g^{-1} at 1 A g^{-1}) and good energy density (29.30 Wh kg^{-1} at power density of 279.78 W kg^{-1}) supported the potential of materials for using as a high-performance supercapacitor.

1.4 Objective

To study the possibility of preparing carbon materials from hydrothermal carbonization of water hyacinth

CHAPTER 2

RESERCH METHODOLOGY

2.1 Chemicals and materials

1. Ferric (III) chloride hexahydrate (FeCl3·6H2O, 99.0%) was purchased from Loba Chemie.
2. Potassium Hydroxide (KOH) (85.0%) was purchased from Merck.
3. Tetracycline (TC) was purchased from Sigma-Aldrich.
4. Carbon black were purchased from Sigma-Aldrich.
5. Polytetrafluoroethylene (PTFE) 60 wt % dispersion in H_2O was purchased from Sigma-Aldrich.
6. Methylene blue (MB) was purchased from Unilab.
7. Methyl orange (MO) was purchased from Unilab.
8. Water hyacinth (Eichhornia crassipes) was obtained from a canal in residential area at Khuan Ru, Rattaphum District, Songkhla province, Thailand (7°11'15.7"N 100°18'58.5"E)

2.2 Equipment and instruments

1. N_2 adsorption-desorption technique (Micromeritics, ASAP 2460)
2. Transmission electron microscopy (TEM, JEOL JEM-2010 and JEOL JEM-2011)
3. Scanning Electron Microscopy equipped with energy dispersive X-Ray Spectroscopy (SEM-EDS, FEI, Apreo).
4. X-ray diffractometer (XRD, Philips, X'Pert MPD).
5. X-ray photoelectron spectroscopy (XPS, Kratos Analytical Ltd., AXIS Ultra DLD)
6. Vibrating-sample magnetometer (VSM, LakeShore, Model 7404,)
7. Thermogravimetric analysis (TGA, Perkin Elmer, TGA7)
8. Inductively Coupled Plasma Optical Emission Spectrometer (ICP-OES, Perkin-Elmer, Avio500)
9. UV-Vis spectrophotometer (Shimadzu, UV1800)
10. Shaking incubator (Sci Finetech, FTSH-501)
11. Potentiostat (Bio-Logic, VSP-300)

2.3 Method

2.3.1 Hydrothermal carbonization of Water hyacinth

The fresh WH stems collecting from residentiary section at Khuan Ru, Rattaphum District, Songkhla province, Thailand (7°11'15.7"N 100°18'58.5"E) were

washed by tap water to remove dirt and impurities. Then the clean WH stems were cut into small pieces (approximately 1X5 cm) and dried in hot air oven at 90°C until the WH sample was completely dried. Next, the pieces of WH stem were ground into fine powder (<710 µm). Afterwards, 8.0 g of dried WH powder was mixed with 150 ml DI water in 400 ml Teflon container and the reaction was conducted at 180°C for 24 hours in 400 ml Teflon-lined stainless-steel autoclave. After cooling down the autoclave naturally, the obtained sample was filtered *via* vacuum filtration to separate the solid and liquid product.

2.3.2 Preparation of magnetic carbon composite from HTC solid product

The obtained solid product or hydrochar was dried at 90°C for 18 hours and labeled as WHHTC. To add the magnetic property, 2.50 g of WHHTC was stirred in 25 ml $FeCl_3 \cdot 6H_2O$ solution for 1 hours. Then 25 ml 10%w/v KOH solution was added dropwise to the mixture and further stirred for 12 hours. Then the mixture was dried at 90°C for 18 hours and carbonized under N_2 atmosphere at 800°C for 3 minutes (ramp rate: 2°C min^{-1} to 600°C holding for 15 minutes and heating 5°C min^{-1} to 800°C holding for 90 minutes). The carbonized sample was further washed by hot DI water several times to remove the impurities and dried at 80°C for 12 hours. The as-synthesized magnetic materials were labeled as MWHHTC(X)-Y where X (X = 0.2 and 1) stand for the ratio of KOH to biochar and Y (Y = 500 and 700) is the carbonization temperature. The conditions using for preparing magnetic carbon materials in this study were shown in the following Table 1.

Table 1 the weight ratio of WHHTC:KOH and synthesis temperature using in this study

Samples	Weight ratio of WHHTC: $FeCl_3 \cdot 6H_2O$: KOH	Carbonization temperature (°C)
MWHHTC(0.2)-500	5:1:1	500
MWHHTC(0.2)-800	5:1:1	800
MWHHTC(1)-500	5:1:5	500
MWHHTC(1)-800	5:1:5	800

2.3.3 The stability of magnetic carbon materials towards various pH range

The magnetic carbon material was studied the iron leaching in various pH to confirm the stability of the material. 0.01 g of magnetic carbon material was shaking in

20 ml pH-adjusted DI water which adjusted the pHs by adding 0.1 M HCl or 0.1 M NaOH. The mixtures were shaken at 250 rpm for 24 hours. Afterwards, the carbon material was isolated from the solution by vacuum filtration. The concentration of iron in the solutions were determined using Inductively Coupled Plasma Optical Emission Spectrometer (ICP-OES).

2.3.4 The adsorption study of magnetic carbon materials

All magnetic carbon materials were roughly tested their adsorption property by immersing 0.01 g sample in 20 ml 500 mg/l MB solution shaking at 250 rpm for 24 hours. Then the adsorbents were separated from the solutions by external magnet. The after-adsorption solutions were determined their concentration by UV-Vis spectrophotometer using calibration method to achieve the optimum adsorption condition. Furthermore, all the adsorption studies were performed using Methylene Blue (MB, a cationic dye), Methyl Orange (MO, an anionic dye) and Tetracycline (TC, a neutral antibiotic) as the model adsorbates which their chemical structures are shown in Figure 2

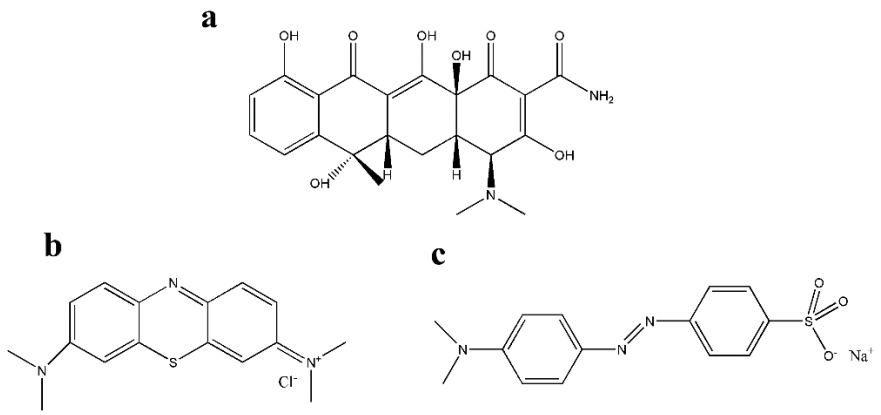

Figure 2 the chemical structure of adsorbates using in this study: (a) Tetracycline (b) Methylene Blue (c) Methyl Orange

2.3.4.1 Adsorption kinetic study

To study the kinetic behavior of the materials, 0.01 g of magnetic carbon material was shaken in 20 ml model dye solution (500 mg L^{-1} for MB and MO, and 200 mg L^{-1} for TC) at room temperature (30±2°C) for 0.5-24 hours using 250 rpm by Shaking incubator. Afterwards, the solutions wes separated by external magnet to investigate

their concentration *via* UV-Vis spectrophotometer. The adsorption capacity in varied time was calculated by equation 6

$$q = \frac{(C_0 - C_e)V}{m} \quad (6)$$

2.3.4.2 Adsorption isotherm study

The adsorption equilibrium behavior was study by adding 0.01 g magnetic carbon into various concentration of adsorbates (50-500 mg L^{-1} for MB and MO, and 40-200 mg L^{-1} for TC). The 50 ml conical flasks containing adsorbate and adsorbent were continuously shaken for 24 hours at 30±2°C. After adsorption, the external magnet was used for separating carbon material from the solution and using UV-Vis spectrophotometer to analyze the concentration of the adsorbates.

2.3.5 The synthesis of supercapacitor using liquid product from HTC method

The HTC liquid product was dried at 80°C for 18 hours so call Crude Liquid Phase or CLP. 1.0 g of CLP was dissolved in 25 ml 2.4 %w/v of KOH solution and stirred for 30 minutes. The CLP-KOH solution was poured into petri dish and cured at 80°C for 18 hours. Then the dried sample was further pyrolyzed under N_2 atmosphere at 800°C for 3 hours using the same ramp rate as magnetic carbon material synthesis. The after-carbonized carbon material was rinsed with 0.1 M HCl and DI water several time to remove alkaline salts and other impurities. In the following step, the sample was dried at 80°C for 8 hours and labeled as CLP+KOH-800.

2.3.6 Fabrication of supercapacitor electrodes from carbon materials derived from CLP and its electrochemical properties

The electrochemical properties of CLP+KOH-800 were tested in a symmetric configuration using free-standing carbon electrodes and 6 M KOH as electrolyte. The free-standing carbon electrodes were fabricated by mixing 90 wt% of CLP+KOH-800 with 5 wt% of Carbon black Super P® Conductive (99+% - metals basis, Alfa Aesar) and 6 wt% of PTFE (polytetrafluoroethylene preparation diluted 10 times with water from a commercial PTFE - 60wt % dispersion in H_2O, Sigma-Aldrich) in absolute ethanol. Ethanol was completely removed from the mixture by heating at 110 °C. Then 2-3 drops of ethanol were added into the dried carbon-binder mixture, pasted between the polyamide sheet and progressively calendered in an electric 2-rolls mill, until a homogeneous film of 100 μm thickness was obtained. The electrodes were punched

in disks of 7 mm diameter and dried at 200 °C overnight. The density of the electrodes was calculated using the following equation:

$$\rho = \frac{m_{electrode}}{V_{electrode}} = \frac{m_{electrode}}{S \cdot t} \quad (7)$$

Where $m_{electrode}$ (g) is the weight of one electrode, $V_{electrode}$ (cm^3) is the macroscopic volume of the electrode, as determined by multiplying the section S (cm^3) and the thickness t (cm). The density of 0.47 g cm^3 was found to be one of the most dense carbons compared to most bio-based activated carbons found in the literature[43]–[46]. This can be explained by the low ratio KOH:carbon precursor used in this experiment.

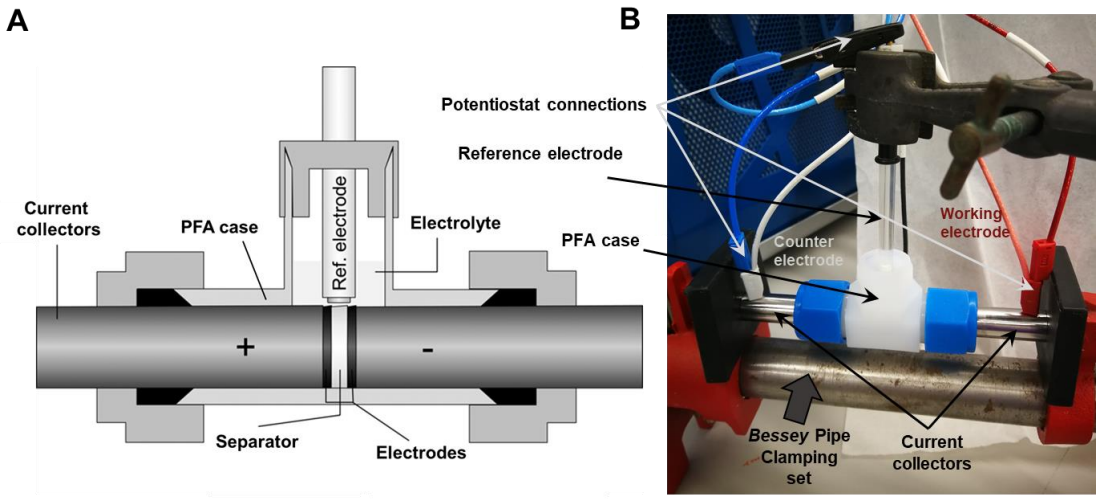

Figure 3 (a) Section of a Swagelok cell (taken from M. Karthik et al [1]) (b) Picture of the electrochemical cell.

The symmetric supercapacitor was built in a *Swagelok T-cell*, by sandwiching the two carbon electrodes (with a weight difference <10%) between two stainless-steel current collectors (Hasteloy® 276) and separated by a 10 mm disc glass fiber separator (Whattman, 1 mm thickness). Prior to the assembly, the two carbon electrodes were wetted with the electrolyte. The polarization of both electrodes could be observed by adding a reference electrode (Calomel electrode, Hg_2Cl_2, in saturated KCl solution) in the T-cell (see Figure 3). The voltage window of the cell was determined by performing CVs at 5mV s^{-1} on the T-cells without carbon electrodes. The corrosion current was only observed beyond 1.3V and 1.2V was thus taken as voltage window (see Figure 4). For the measurements, the *T-Cell* was connected to a VSP Biologic potentiostat. Furthermore, 500 cycles galvanostatic charge-discharge

experiment were run at 5 A g^{-1} before the other electrochemical analysis to improve the accessibility of electrolyte to the material. Cyclicvoltammetry (CV) were performed using various scan rates from 5 mV s^{-1} to 2 V s^{-1}. The Galvanostatic charge discharge (GCD) of supercapacitor was achieved using different current densities from 0.1 to 130 A g^{-1}. Moreover, the electrochemical impedance spectroscopy (EIS) in frequency range of 200 kHz and 10 mHz was performed with a signal amplitude of 10 mV. The specific capacitances (F g^{-1} and F cm^{-3}) of a working electrode were calculated from the CVs, GCDs and EIS using the equations:

$$C_{CV} = \frac{4.I}{v.X} \quad (8)$$

$$C_{GCD} = \frac{4.Q}{(\Delta V - IR_{drop}).X} \quad (9)$$

$$C_{EIS} = \frac{4.|Z''(\omega)|}{2\pi\omega(Z'(\omega)^2 + Z''(\omega)^2).X} \quad (10)$$

Where I represents the current in unit of mA. V is the scan rate (mV/s) using in the cyclo-voltammetry experiment. Q (C) is the electric charge derived from the discharge cycle of galvanostatic charge-discharge experiment. ΔV (V) is the voltage window. IR_{drop} (V) represents the voltage drop during GCD. For EIS study, **ω**(Hz) stands for the frequency using in the system, while Z'(**Ω**) and Z"(**Ω**) are the impedance in real part and imaginary part occurred in the system. Finally, for calculating gravimetric capacitance, X is the mass of the working electrode in unit of grams. While X presents the electrode volume in cm^3 in case of volumetric capacitance.

2.3.7 The Carbon materials characterization

1. N_2 adsorption-desorption technique was used for study the porosity and pore texture of the as-synthesized materials. Before performing the analysis, the samples were degassed at 200°C for 900 minutes.
2. Transmission electron microscopy was used for investigating nanosized materials including character of iron in the samples.
3. Scanning Electron Microscopy equipped with energy dispersive X-Ray Spectroscopy (SEM-EDS) was used to study the surface morphology and iron distribution in magnetic adsorbents

4. X-ray diffractometer was used to identify the iron species of magnetic carbon materials.
5. X-ray photoelectron spectroscopy (XPS) was used to study surface functionality and elemental composition of the materials.
6. Vibrating-sample magnetometer (VSM) was used to analyze the magnetism of the materials.
7. Thermogravimetric analysis (TGA) was used to identify the thermal stabilities of the liquid product from HTC process.

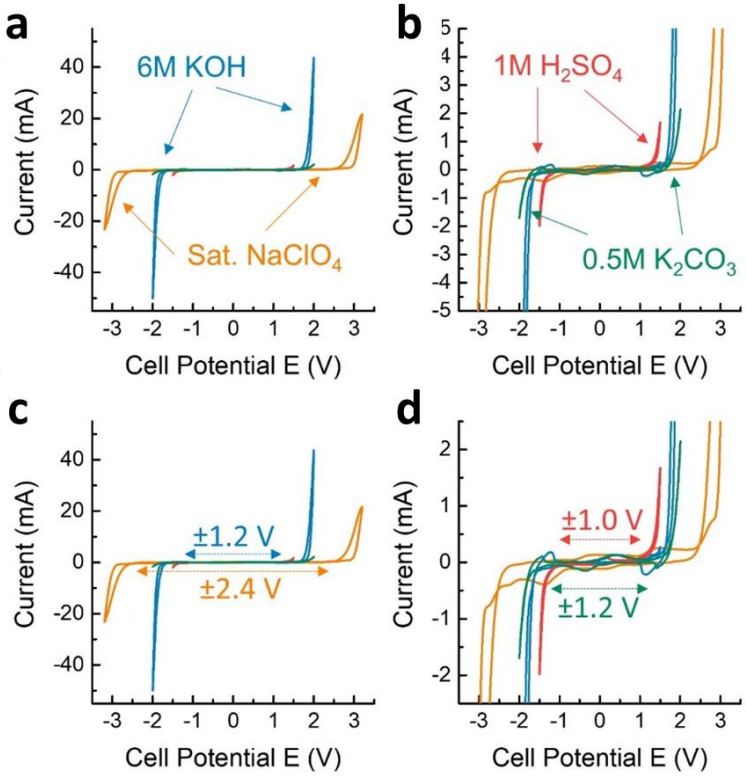

Figure 4 Electrochemical stability window of 6MKOH compared to other electrolytes (1M H_2SO_4, 0.5M K_2CO_3 and saturated $NaClO_4$). (a) and (b), Cyclovoltammograms showing the corrosion or degradation current peaks observed at various potentials; (c) and (d) Cyclovoltammograms showing the stable electrochemical potential window chosen for each electrolyte. It is seen that 6M KOH allows a voltage window of 1.2 V while avoiding electrolyte degradation at high overpotential.

CHAPTER 3

RESULT

3.1 Character of hydrothermal carbonization products

The hydrothermal carbonization of water hyacinth at 180°C for 24 hours provided both solid and liquid products. The solid phase (WHHTC) appeared dark brown and had approximately 46.34±2.88 wt% yield compared with the dried water hyacinth precursor. The obtained liquid product was a dark brown solution. This fraction was dried and weighed in order to calculate %yield of the product. The approximate %yield of dried crude liquid phase product (herein called CLP) was found to be 16.86±2.02 wt% with respect to the dried WH precursor, which was further employed as a carbon precursor for the production of supercapacitors. The overview of the synthesis is shown in Scheme 1.

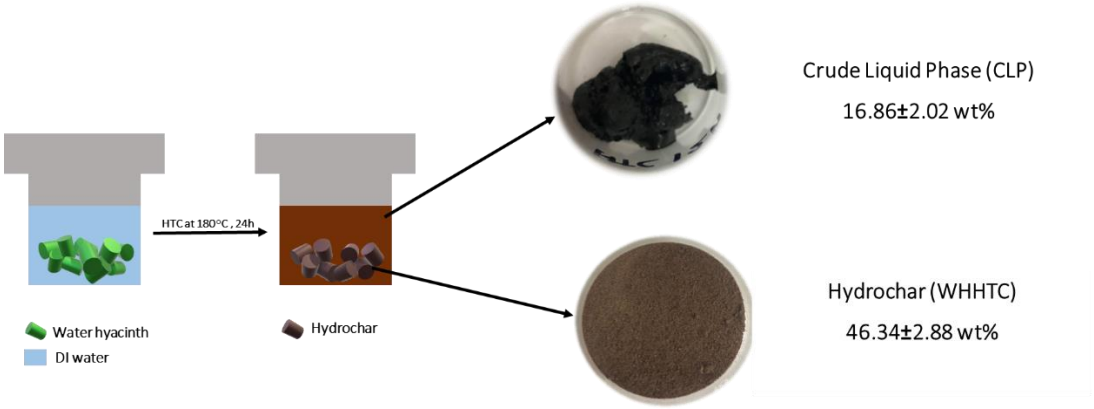

Scheme 1 the material preparation steps *via* hydrothermal carbonization of water hyacinth at low temperature

The surface chemical functionality and elemental content of WHHTC, the obtained hydrochar, was investigated by XPS. The result in Table 2 suggests that even before simultaneous magnetization and activation, WHHTC has rather satisfactory carbon (65.80 wt%) and oxygen (27.63 wt%) contents.

Furthermore, the C 1s deconvolution spectra of WHHTC in Figure 5 also show that the material main functional group is C=C (43.3 %Area) followed by C-O-C (22.2 %Area), C-O (14.0 %Area), C=O (14.0 %Area), and O-C=O (6.4 %Area) as shown in Table 3.

Table 2. Elemental compositions of prepared carbon materials characterized by XPS.

Materials	wt%						
	C	O	N	Ca	Si	Mg	Cl
MWHHTC	65.80	27.63	1.84	2.75	1.95	-	-
MWHHTC(1)-800	76.45	16.44	-	7.10	-	-	-
CLP	60.82	24.60	4.73	2.93	1.34	2.59	2.98
CLP+KOH-800	78.73	15.05	-	-	6.22	-	-

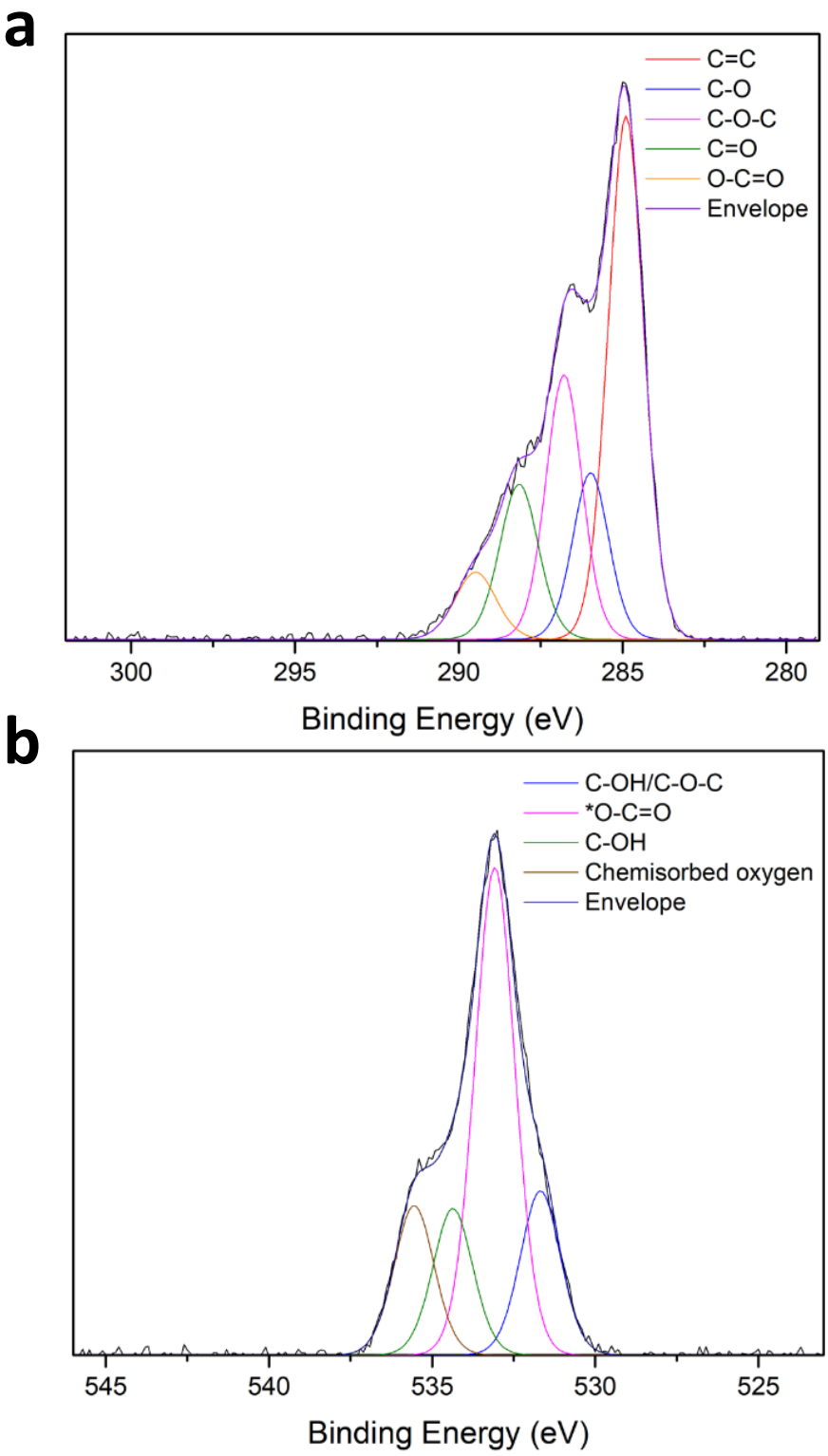

Figure 5 (a) the C1s and (b) deconvolution spectra of WHHTC

Table 3. %Area of functional groups derived from C1s deconvolution XPS spectra of prepared materials.

Materials	%Area					
	C=C	C-O	C-O-C	C=O	O-C=O	π—π*
MWHHTC	43.3	14.0	22.2	14.0	6.4	-
MWHHTC(1)-800	65.5	16.7	6.8	4.6	4.0	2.4
CLP	43.3	14.0	22.2	14.0	-	-
CLP+KOH-800	64.9	16.6	8.4	5.2	5.0	-

Despite the rich oxygenated chemical functionality in the WHHTC, it has a relatively poor surface area (7.35 m^2/g) and terribly small amount of pore volume (0.0440 cm^2/g) as shown in Table 4.

Table 4. BET surface area, total pore volume micropore volume and mesopore fraction of prepared materials.

Materials	BET surface area ($m^2\ g^{-1}$)	Total pore volume ($cm^3\ g^{-1}$)	micropore volume ($cm^3\ g^{-1}$)	mesopore fraction (%)
MWHHTC	7.35	0.0440	0.0006	98.64
MWHHTC(1)-800	973.56	0.6217	0.0888	85.71
CLP-800	144.70	0.0849	0.0311	62.64
CLP+KOH-800	2544.87	1.4563	0.0889	93.90

The thermal behavior of CLP was studied in detail at temperature range 50-1000°C (ramp rate = 10°C min^{-1}) under N_2 atmosphere by TGA. According to the thermogram in Figure 6, the weight remained 48.30 wt% even at 1000°C. The thermogram of CLP apparently exhibits 32.4 wt% loss around 200-700°C. Above 700°C, there is a minor weight loss by 19.3 wt%.

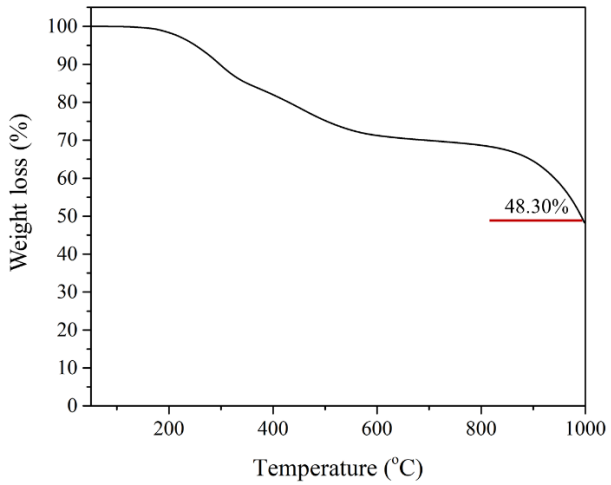

Figure 6. TGA thermogram of CLP. The experiment was performed from 50-1000 °C (ramp rate: 10 °C min^{-1})

Moreover, the lignin content of CLP was examined using the TAPPI T222 om-98 standard method[47] and found to be 5.33 wt%.

The chemical functionality of CLP investigated using XPS (Table 2) indicates that major elements of CLP were carbon, oxygen, and nitrogen at 60.82 wt%, 24.60 wt%, and 4.73 wt%, respectively. Hence, CLP from green HTC of water hyacinth composed of high proportion of carbon (mainly sp^2 carbon (43.3%) and C-O (14.0%)) (Table 3).

3.2 Magnetic carbon materials as an adsorbent

3.2.1 Characterization of magnetic carbon materials

The adsorption of initially 500 mg L^{-1} methylene blue was tested with all as-prepared magnetic carbon materials to select near optimal synthesis conditions for an adsorbent.

On preparing magnetic carbon materials, we employed 500 or 800 °C to study effects of this choice on magnetization degree and porosity properties of the resulting carbons. It is clear that both carbonization temperatures (500 °C and 800 °C) and KOH weight ratio (biochar (WHHTC): KOH = 1:1 and 1:0.2) had no effects on the magnetic properties, as observed by the tiny differences in magnetizations shown in Table 5 (all in the small range 4-6 emu g^{-1}). Nonetheless, both factors significantly influenced porosity (Table 5). Therefore, MWHHTC(1)-800 was selected for further characterization and adsorption studies, having both largest surface area and pore volume among the cases tested.

Physicochemical properties, including surface area and pore texture of MWHHTC(1)-800, were studied in detail by various techniques. Figure 7a shows the N_2 isotherm of MWHHTC(1)-800, which clearly is of type IV with an obvious hysteresis loop. This indicates that the material contained mesopores, which is further confirmed from the narrow pore size distribution (PSD) in the range ~1.5-5.0 nm (Figure 7b). Furthermore, MWHHTC(1)-800 possessed high specific surface and large porosity, 973 m^2/g and 0.62 cm^3/g respectively. The material also had high mesoporosity, 87% of the total pore volume (Table 5).

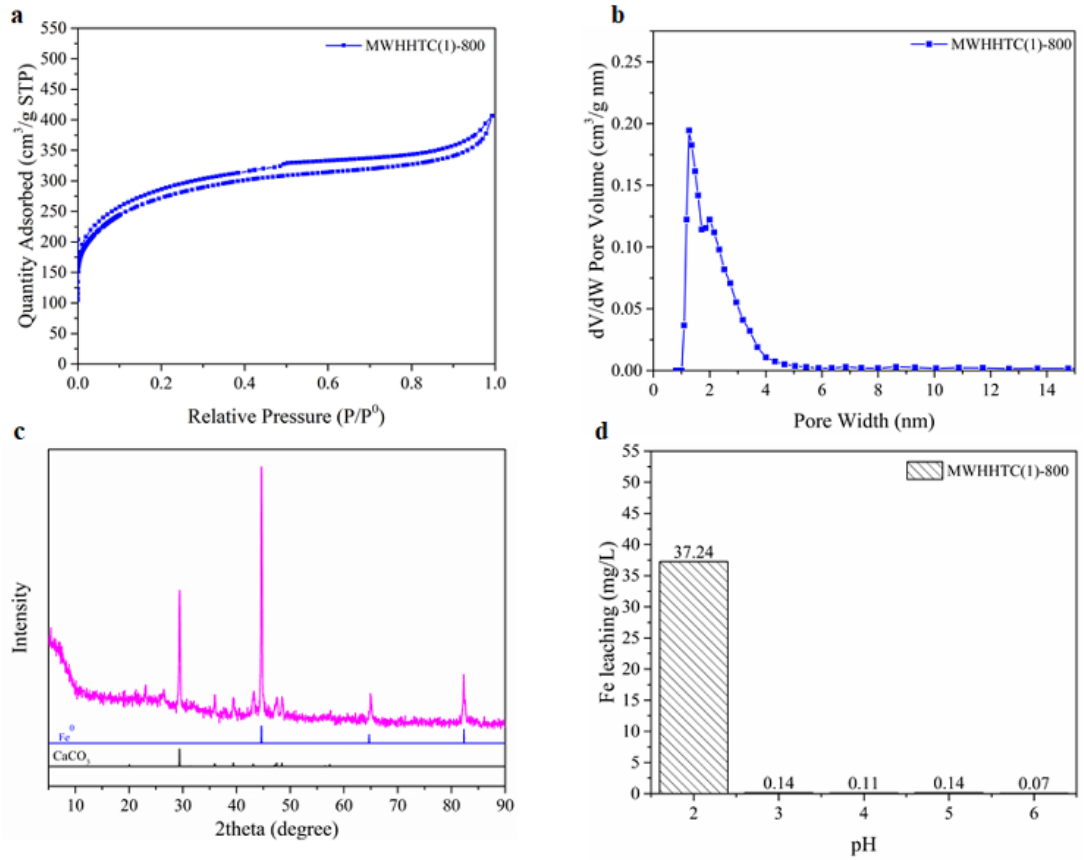

Figure 7. (a) N_2 sorption-desorption isotherm, (b) pore size distribution calculated by DFT, (c) XRD pattern, and (d) leached iron concentrations at various pHs, for MWHHTC(1)-800.

Table 5. Comparison of magnetization, porosity parameters and MB adsorption capacity across various ratios of activating agent to magnetic adsorbent.

Materials	Magnetization (emu g^{-1})	Specific surface area (m^2 g^{-1})	Total pore volume (cm^3 g^{-1})	mesopore fraction (%)	$q_{t=24h}$ on MB (mg/g)
MWHHTC(0.2)-500	6.00	271.12	0.1825	60.33	16.46
MWHHTC(0.2)-800	4.81	677.66	0.4348	56.28	184.24
MWHHTC(1)-500	6.00	398.14	0.2296	50.57	10.60
MWHHTC(1)-800	4.11	973.56	1.5253	87.89	535.31

To investigate the changes in elemental composition and functionality both qualitatively and quantitatively, XPS measurements were carried out on both non-magnetic hydrochar (WHHTC) and the selected magnetic material (MWHHTC(1)-800). The C 1s XPS spectra of both WHHTC (Figure 8a) and MWHHTC(1)-800 (Figure 8b) reveal sp^2 carbon as the major peak, with 284.6 eV binding energy (BE). The gained sp^2 carbon content in MWHHTC(1)-800 was clear from those spectra. The C=C functional group in MWHHTC(1)-800 was significantly increased by carbonization and magnetization of relative to initial non-magnetic biochar (WHHTC), from 43.3% to 65.5%, in accordance with the decrease in oxygen content (Table 2). The peaks at BE 286.0 and 286.8 eV correspond to C-O and C-O-C bonds, respectively. The peaks at 288.1 and 289.4 eV confirm the presence of C=O and O-C=O groups. While the content of C=C (sp^2) increased, there is decreasing of oxygen functionalities intensity in MWHHTC(1)-800.

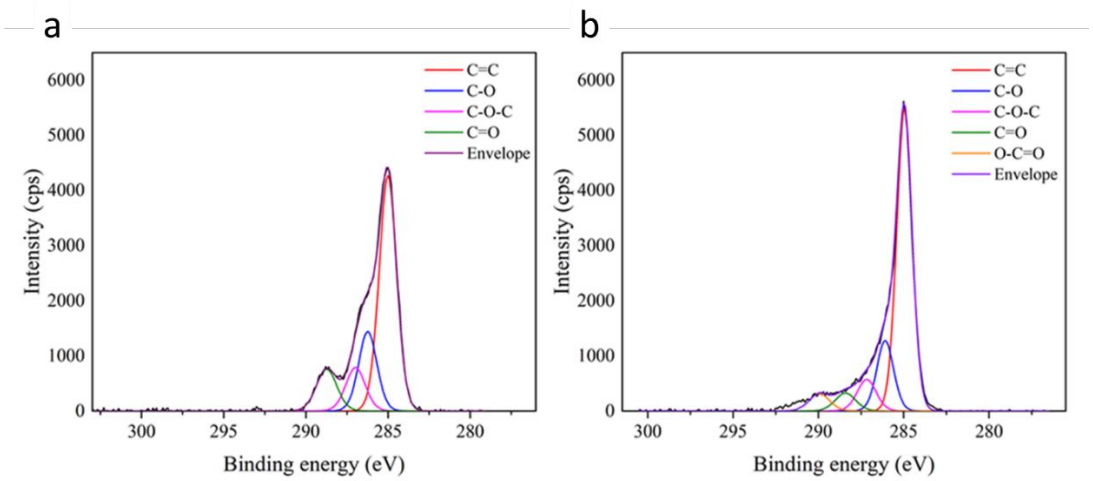

Figure 8 XPS C1s spectra of (a) WHHTC and (b) MWHHTC(1)-800.

Iron occupancy and iron particles in MWHHTC(1)-800 magnetic carbon material were characterized by XRD, TEM, and SEM-EDS techniques, as shown in Figure 7c and Figures 9a-f, respectively. X-ray diffraction pattern of MWHHTC(1)-800 in Figure 7c had peaks at 2θ of 44°, 65° and 82°, corresponding to (110), (200) and (211) planes of zero-valent iron (ICDD 00-001-1262). Furthermore, the diffraction pattern also indicates a small amount of calcium carbonate residue (ICDD 01-072-1937), which corresponds to the small calcium content detected by XPS.

TEM images in Figures 9a-b confirm the presence of iron particles embedded uniformly throughout the material, which is in accordance with the SEM-EDX results in

Figure 6f. The SEM-EDX technique also reveals the proportions of carbon, oxygen and iron as 74.6 wt%, 12.6 wt% and 6.9 wt%, respectively.

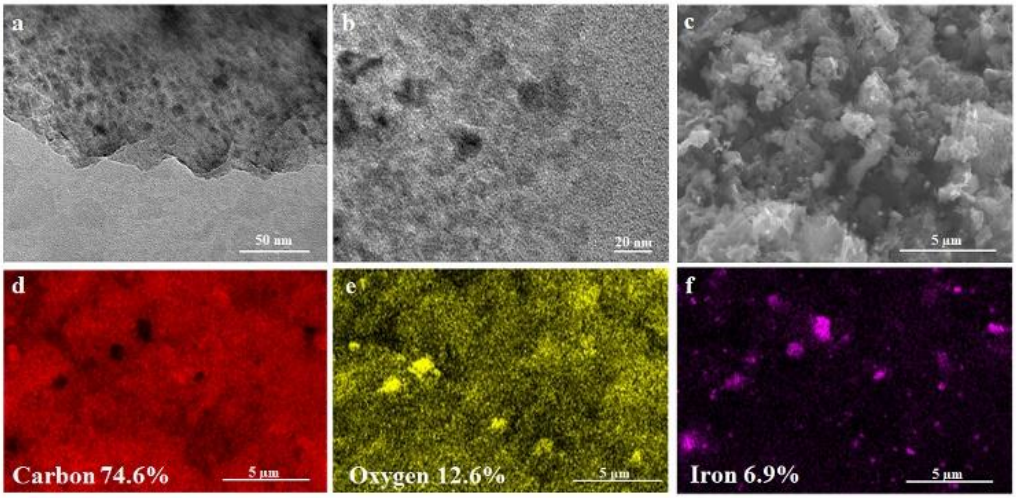

Figure 9 (a-b) TEM images, (c) SEM image, and (d-f) EDX mappings of MWHHTC(1)-800.

The stability of iron particles in composite adsorbents against leaching over a wide pH range is important for eventual practical applications. MWHHTC(1)-800 was tested at various levels of pH (2.05-6.30) for 24 hours. The results in Figure 7d indicate that MWHHTC(1)-800 had good magnetic stability over a wide pH range from acidic (pH 3.05) to neutral (pH 6.30), with negligible release of iron from the composite (<0.15 mg/L). In particular, at the pH of DI water (pH 6.30), only 0.07 mg/L of Fe ions was released. However, the Fe ion concentration became higher in acidic conditions (pH 2.05).

3.2.2 Adsorption performance of magnetic carbon material MWHHTC(1)-800

The adsorption kinetics plots in Figure 10a show that the adsorption rapidly reached equilibrium, within only 300 minutes even at extremely high concentration of MB (500 ppm), MO (500 ppm) or TC (200 ppm).

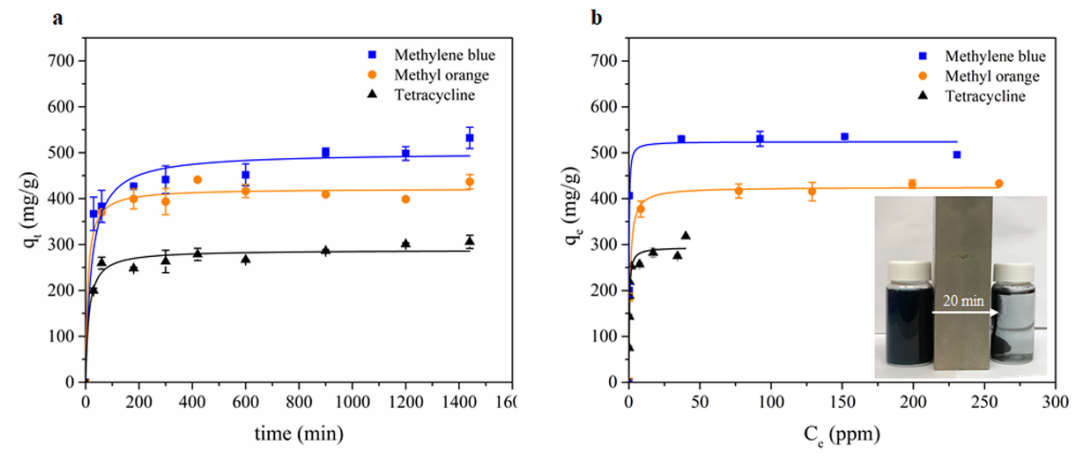

Figure 10 (a) Adsorption kinetics and (b) adsorption isotherms of MB, MO, and TC adsorption by MWHHTC(1)-800.

In order to investigate the kinetics of adsorption in detail, the experimental data were fitted with a pseudo second order model as shown in equation 11

$$q_t = \frac{k_2 q_e^2 t}{1 + k_2 q_e t} \tag{11}$$

Here q_t is adsorption capacity at any time t, and k_2 is a rate constant in the pseudo-second-order model. The calculated rate constants (k_2) for all adsorbates are fairly high, as shown in Table 6.

Furthermore, equilibrium adsorption isotherms were determined experimentally. The isotherms in Figure 7b show that the MWHHTC(1)-800 had high adsorption capacity of MB, MO and TC. The maximum capacities were estimated by fitting the Langmuir isotherm model shown in equation 12

$$q_e = \frac{q_{max} \cdot K_L \cdot C_e}{1 + K_L \cdot C_e} \tag{12}$$

Here q_{max} is maximum adsorption capacity and K_L is Langmuir constant. The isotherm data was well fit by the Langmuir model (R^2 = 0.90041, 0.99781, 0.93822). and the Langmuir parameters and the maximum adsorption capacities by MWHHTC(1)-800 of MB, MO and TC are summarized in Table 6.

Table 6 Pseudo second kinetic and Langmuir parameters of MWHHTC(1)-800 on MB, MO and TC adsorption.

Adsorbate	Pseudo second kinetic model			Langmuir model		
	k_2 (g (mg min)$^{-1}$)	q_e (mg g^{-1})	R^2	K_L (L mg^{-1})	q_{max} (mg g^{-1})	R^2
Methylene blue	9.14x10^{-5}	500.41	0.99806	5.6447	524.20	0.90041
Methyl orange	2.73x10^{-4}	421.61	0.99913	1.1772	425.15	0.99781
Tetracycline	2.82x10^{-4}	288.00	0.99926	2.7576	294.24	0.93822

3.3 Carbon-based supercapacitor prepared from the crude liquid phase (CLP)

3.3.1 Characterization

In this study, only a small amount of KOH (CLP:KOH = 1:0.6 by weight), relative to other reported studies[7,46], was mixed directly into CLP solution that was further pyrolyzed, to enhance porosity without a pretreatment step.

A carbon- based supercapacitor prepared with KOH activated CLP had an extremely large BET specific surface area of $2365.50 \pm 163.70\ m^2/g$ and large porosity around $1.29 \pm 0.15\ cm^3\ g^{-1}$. The sample preparation was carried out in triplicate to confirm reproducibility of the preparation protocol. Due to uniformity of the mix with KOH in the activation step, surface area and pore volume were similar in all replicates along with pore texture, as indicated by the small standard deviations. Furthermore, the N_2 sorption-desorption isotherms for all replicates were of mixed type I and IV, in the IUPAC classification of isotherms, indicating micropores or small mesopores that are suitable for electrochemical applications due to high diffusivity of the electrolyte[20]. One isotherm from the replicates is shown in Figure 11a.

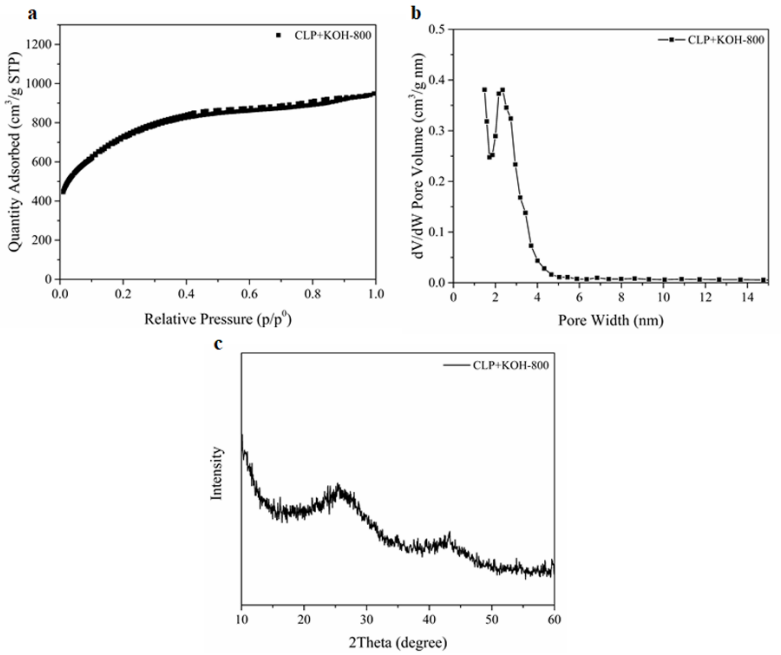

Figure 11 (a) N_2 sorption-desorption isotherm, (b) pore size distribution calculated by DFT, and (c) XRD pattern of CLP+KOH-800.

Chemical functionality and elemental composition of CLP+KOH-800 were investigated by XPS technique and compared to those of pristine CLP (Tables 2 and 3). The activation at 800 °C increased the carbon content of CLP+KOH-800 from 60.82 wt% to 78.73 wt%, while the oxygen content dropped to 15.05 wt%. Moreover, sp^2 carbon content significantly increased from 43.3 wt% to 64.9 wt%, so abundant π aromatic components were present in the activated sample. Evidence of sp^2 carbon is also found in the XRD pattern in Figure 11c.

The XRD result shows two broad diffraction peaks at 2θ = 26° and 44°, corresponding to (002) and (100) planes in turbostratic carbons. The low intensity broad diffraction peaks suggest a low degree of graphitization in the CLP+KOH-800 material, in comparison to pure graphite.

3.3.2 Electrochemical properties and recycling test

The super-capacitive performances of CLP+KOH-800 were investigated using cyclic voltammetry (CV), galvanostatic charge-discharge (GCD) and electrochemical Impedance Spectroscopy (EIS).

The CVs at various scan rates, shown on Figure 12a, reveal the super-capacitive nature of CLP+KOH-800 by showing an important capacitive current characterized by a rectangular CV shape. However, the CVs reveal also two important side phenomena occurring during charging and discharging. The first, related to the important current peak observed at low scan rate (5 and 10 mV s^{-1}), is attributed to carbon corrosion/oxidation. The second phenomenon, called pseudo-capacitance, is characterized by the current bumps at low over potentials during the charging and the constant negative current slopes during the discharge.

In order to assess the performance of the materials at different rates, the capability of the material was calculated from the CVs and shown on Figure 12b. Both gravimetric and volumetric performances reveal that the material exhibits good rate capability, maintaining 80% of its capacitance at 2 V s^{-1} and 80 F g^{-1} at 100 A g^{-1} as determined by GCDs (see Figure 13).

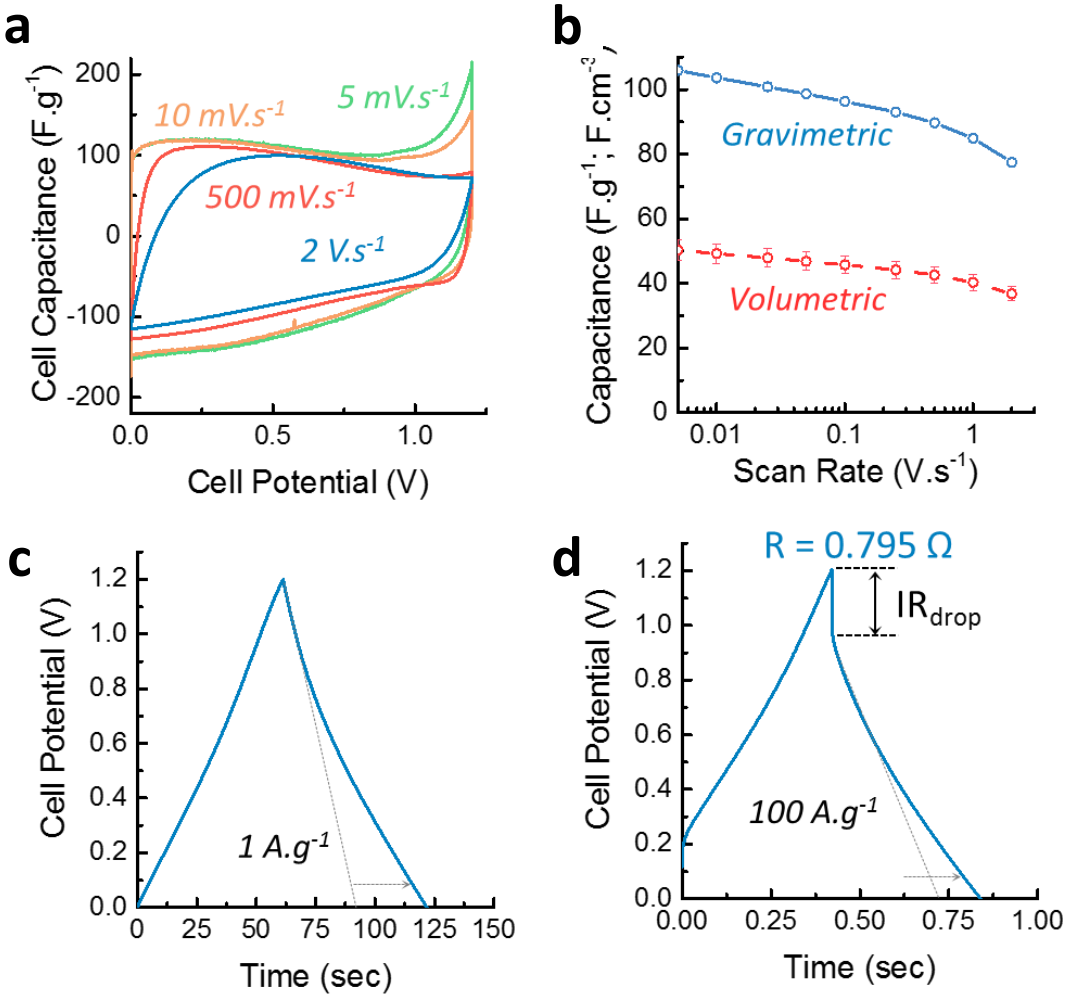

Figure 12 (a) Cyclic voltammograms (CV) of the symmetric cell at various scan rates; (b) Rate capability of the device extracted from the CV curves and corresponding error bars due to the incertitudes on the electrode density measurement; (c)&(d) Galvanostatic charge discharge curves at 1 A g^{-1} and 100 A g^{-1} and the corresponding IR_{drop} measurement.

The galvanostatic charge/discharge also confirm the supercapacitive and pseudo-capacitive behaviour of CLP+KOH-800 by exhibiting a nearly triangular shape at 1 A g^{-1} and 100 A g^{-1} (Figure 12c, d). The increase in charge and discharge time due to the faradaic charge transfer is indicated by the dotted arrow which compare the performances with an "ideal" double layer supercapacitor. Additionally, the small iR_{drop} in the GCD profiles indicate good electrical conductivity and low cell resistance of 0.795 **Ω**.

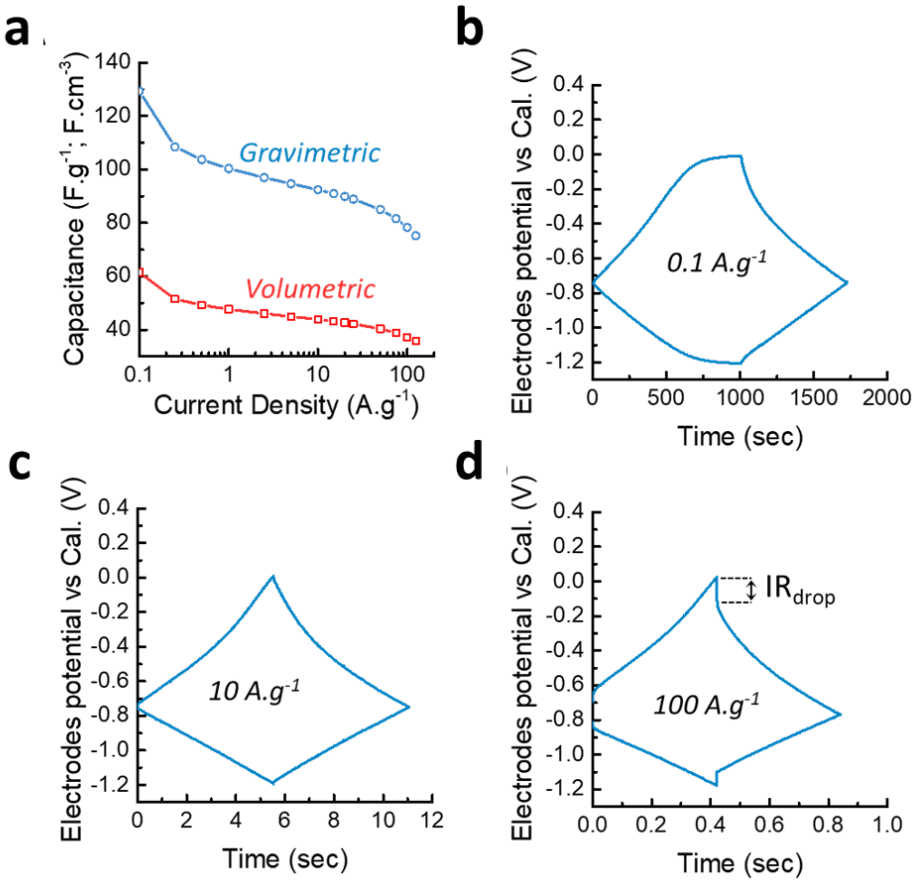

Figure 13 Electrochemical tests in 6M KOH. (a) Capability of the material calculated from the galvanostatic charge/discharge curves (GCDs); (b,c,d) Simultaneous polarization of the working and the counter electrodes during GCDs at respectively 0.1, 10 and 100 A g^{-1}.

EIS was measured to provide more insight into the charging kinetics of both electrodes before and after the electrodes were cycled to test the stability of the device. The Nyquist plot (Figure 14a) reveals the presence of a semicircle at high frequency (above 100Hz), representing the charge transfer resistance R_{ct} of the faradaic processes occurring during charging and discharging.

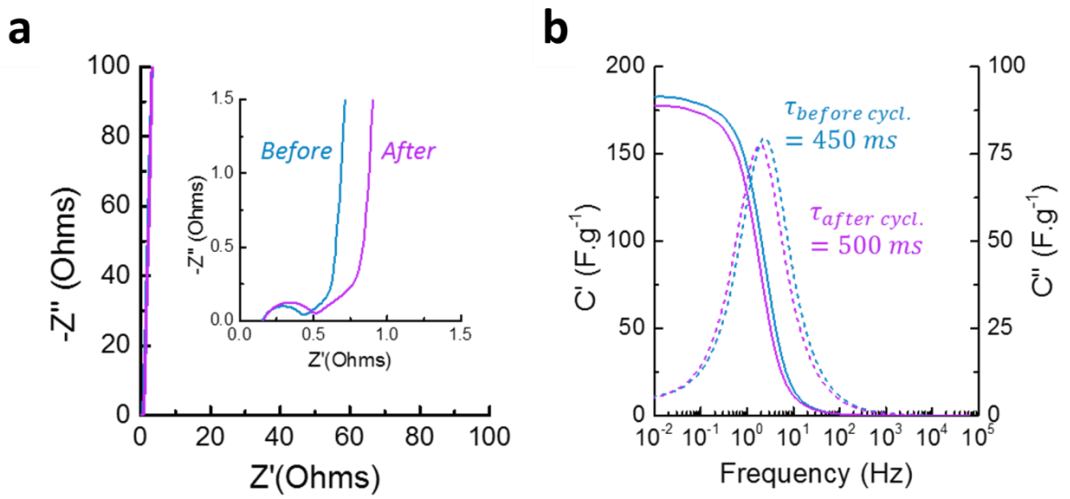

Figure 14 (a) Nyquist plot showing the capacitive and resistive regions and (b) Bode plot showing the real and imaginary capacitance of the material before and after 10,000 cycles of galvanostatic charge/discharge.

Between 100 Hz and 100 mHz, the resistive regime shifts into a capacitive regime where the increase in capacitance is limited by diffusion (*restricted-diffusion* regime), (see Figure 14b). When the frequency passes below 100 mHz, the material becomes fully capacitive and the ions are able to penetrate inside the micropores, creating a vertical line on the Nyquist plot. Here also, it is observed that the ionic diffusion within the mesopores of the materials is not drastically changed upon cycling and the maximum capacitance obtained by EIS is also comparable. By calculating the cyclability from the GCD curves (Figure 15a), a retention of 92% after 10,000 cycles is acceptable and could be increased by reducing slightly the voltage window or choosing a less corrosive electrolyte.

Finally, the Ragone plot (Figure 15b) illustrates both the energy and power density of the material, providing an overview of the materials performances. Despite its relatively low micropore volume and large average pore size, CLP+KOH-800 already exhibits electrochemical gravimetric energy density comparable with commercially

available carbons (~5Wh kg^{-1}) and good power density (~30 kW kg^{-1}) which could be explained by the hierarchical porous structure and the abundance of mesopores.

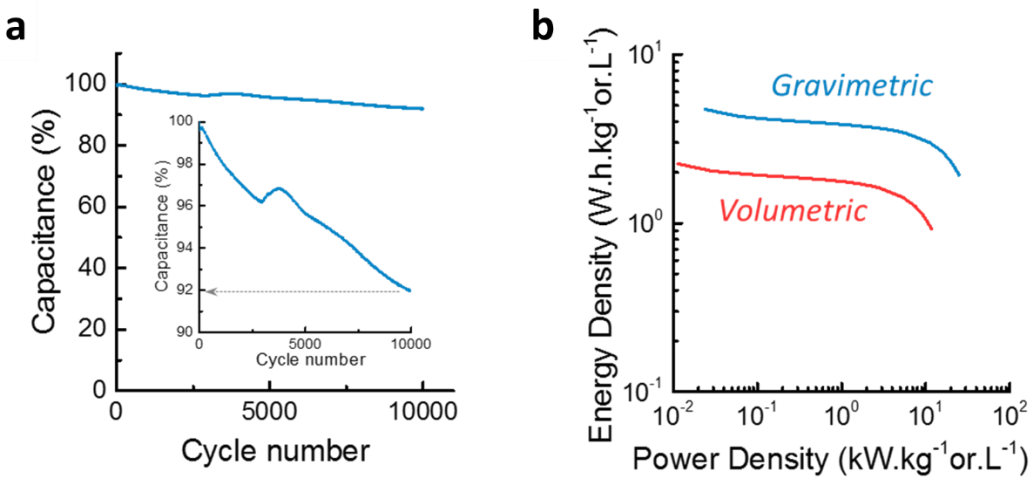

Figure 15 (a) cyclability over 10,000 cycles at 10 A g^{-1} and (b) Ragone plot.

CHAPTER 4

DISCUSSION

4.1 Hydrothermal carbonization product characterization

4.1.1 Solid phase

As mentioned in chapter 3, the solid phase or WHHTC has rather low surface area which is inadequate for an adsorbent. Therefore, the WHHTC was further activated to improve its porosity and adsorption performance. Moreover, this further activation was simply coupled with *in situ* magnetization to provide the adsorbent not only higher porosity but also magnetic properties.

4.1.2 Liquid phase

In spite of the high yield (20-50 wt%), the extraction of crude liquid from lignocellulosic biomass has usually involved toxic organic solvents[48], [49], an alkaline catalyst[21], [22], [48]or rather high temperatures (>250°C)[48], [50]. Notably, in this current study, HTC was performed at a relatively low temperature (180 °C) with only water as the medium. This unusual choice can reduce energy consumption and the complexity of the system.

Besides the terrific thermal stability of CLP, the thermogram could indicate the lignin consistence in the sample. The 32.4 wt% loss at 200-700 °C, corresponding to decomposition of cross-links. At Over 700 °C, a small 19.3 wt% weight loss from decomposition of lignin[51] is observed. Apart from the excellent thermal stability, this lignin content in CLP also enables solution-consisted procedures[52] making the further preparation of functional CPL-based materials more facile, low-cost and scalable in comparison to the use of solid precursors.

As mentioned in XPS result section, the CLP contained favorable chemical functionalities especially, suitable carbon and oxygen content which giving it good potential for use in synthesis of functional carbon materials.

4.2 The character and adsorption property of magnetic adsorbents

4.2.1 Morphology and character study of the magnetic carbon adsorbents

Considering the magnetic property of the materials, the magnetization of 4.11 emu/g for MWHHTC(1)-800 is comparable to other porous carbon-based materials

reported earlier, such as 3.679 emu g^{-1} for Fe_3C/Fe/C magnetic hierarchical porous carbon[53] and 3.83 emu/g for magnetic chitosan/poly (vinyl alcohol) hydrogel beads[54]. These magnetization values are sufficient to make MWHHTC(1)-800 easily separable from an aqueous suspension with an external magnet.

Furthermore, the MWHHTC(1) -800 exhibited the outstanding specific surface area, pore volume and interesting pore texture by containing 87% of mesopore. This large fraction of mesopores not only improves adsorption rate but also enables adsorption of large molecules[55], such as the adsorbates in this study (MB, MO and TC).

From the XPS and BET result. It indicate that simultaneous magnetization and activation at 800 °C not only improved the porosity but also changed the chemical nature of the carbon product. Moreover, the absence of Fe signal in the wide scan might be caused by the embedding of iron particles deep in the carbon matrix, so they could not be detected by XPS.

The formation of metallic iron starts with $Fe(OH)_3$ from the reaction between $FeCl_3$ and KOH. At ~400 °C, it was converted into Fe_2O_3 and subsequently transformed into magnetite (Fe_3O_4). Above 700 °C, magnetite was reduced to zero-valent iron particles[35]. During the magnetization process, KOH also played a role as an activating agent forming K_2CO_3 and K_2O species, which could react with carbon in the materials above 700°C, increasing porosity[54]. In this study, the material was prepared by carbonization under N_2 atmosphere at 800 °C to accomplish activation and also to obtain magnetic properties. Our method combined magnetization and activation in a single step, without further post-formation of magnetic particles after activation.

It is noticeable that the synthesis of magnetic carbon composite in this work involved no multi-steps, for example the formation of magnetic ion phase either before or after the incorporation of such magnetic iron species into the adsorbents. This could certainly reduce time-consumption and extra chemicals.

Although few publications have reported on Fe leaching from iron-based magnetic composites[56], [57], the magnetic adsorbent (MWHHTC(1)-800) has an outstanding stability over wide range of pH (3.05-6.30). Despite some iron discharge in strongly acidic conditions, the material had outstanding resistance to leaching

compared with prior studies[14], [56], [57] that assessed pH 3.0. This might be a consequence of entrapping the iron particles by the carbon matrix, and matches the absence of iron signal in XPS, as well as entrapped iron particles seen in TEM images. It is worth mentioning that the stability of MWHHTC(1)-800 over a wide pH range facilitates its practical application as superior adsorbent.

4.2.2 The adsorption study of magnetic carbon material MWHHTC(1)-800 on MB, MO and TC removal

The adsorption properties in kinetic term is outperforming a number of carbon-based adsorbents[58], [59]. Only 0.10 g of MWHHTC(1)-800 was added into 15 mL of 500 mg/L MB followed by simple shaking. After shaking for only ~1.5 minutes, the dark blue solution faded in color, indicating that most MB molecules were removed.

After fitting with pseudo second order kinetic model, the high rate constant indicated the rapid adsorption rate. This fast adsorption of all adsorbates tested here can be explained by not only the high specific surface area of MWHHTC(1)-800 but also by the high mesoporosity, which enables rapid adsorption of large molecules like MB, MO and TC in our study[58].

Furthermore, the maximum adsorption capacities by MWHHTC(1)-800 of MB, MO and TC are shown in Table 7. These are high (524.20, 425.15 and 294.24 mg/g for MB, MO and TC, respectively) in comparison with the maximum adsorption capacities of biomass[14], [56], [60] and non-biomass[57], [58] based magnetic adsorbents. The great adsorption capacities achieved can be related to XPS and N_2 sorption-desorption results: MWHHTC(1)-800 had high specific surface, high porosity, and large fraction of mesopores (2-5 nm) providing access for bulky molecules to the pores. As mentioned in XPS interpretation, MWHHTC(1)-800 contains 65.5% sp^2 carbon and all the adsorbate molecules have at least 2 aromatic rings in their structure (Figure 1). This match of adsorbent and adsorbate characteristics enabled $\pi-\pi$ interactions, as a mechanism that boosted the adsorption capacity[59].

Table 7 The comparison of k_2 (pseudo-second model) and q_e (Langmuir model) on MB, MO and TC adsorption between this study and others from literature.

Materials	S_{BET} (m^2/g)	Adsorbate	k_2 (g/ (mg min))	q_{max} (mg/g)	Ref.
Magnetic carbon from mangosteen peels	831.5	Methylene Blue	-	46.296	[61]
Magnetic carbon from corncob	153.89		$3.17x10^{-4}$ at 281.25 mg/L	163.93	[62]
Magnetite silica gel	597.09		$2.81x10^{3}$ at 250 mg/L	246.31	[63]
Magnetic graphene sponge	-		$1.5x10^{-4}$ at 175 mg/L	526	[64]
Amino-functionalized magnetic bacterial cellulose/activated carbon	-	Methyl orange	$1.6x10^{-3}$ at 50 mg/L	98.33	[65]
Carbon dots/$ZnFe_2O_4$	116.8		$2.7x10^{-2}$ at 20 mg/L	181.2	[66]
Magnetic chitosan/poly (vinyl alcohol) hydrogel beads	60.1		$2.86x10^{-2}$ at 30 mg/L	68.86	[54]
Chitosan-based magnetic composite particles	8.48	Tetracycline	$5.25x10^{5}$ at 100 mg/L	67.1	[67]
Magnetic carbon composites from bagasse	43.29		$7.52x10^{-4}$ at 80 mg/L	48.35	[14]
Magnetic carbon adsorbent from water hyacinth	**973.56**	**Methylene blue**	**$9.14x10^{-5}$ at 500 mg/L**	**524.20**	**This work**
		Methyl orange	**$2.73x10^{-4}$ at 500 mg/L**	**425.15**	
		Tetracycline	**$2.82x10^{-4}$ at 200 mg/L**	**294.24**	

4.3 Carbon-based supercapacitor prepared from the crude liquid phase (CLP)

4.3.1 Characterization

Since CLP, derived from liquid HTC product from water hyacinth, is composed of phenolic-like compounds, it has high solubility in polar solvents, especially water. The miscibility with water guarantees that CLP can be easily mixed, homogeneously and thoroughly, with other added substances. In this case, only small amount of KOH was added into the system. It is worth noting that the activation reported here employed much lower KOH amount (1: 0.6 wt% of dried liquid product: KOH) in comparison to conventional activation with solid biomass ($\geq$ 1:1 wt%) and ensured homogeneous mixing of KOH during the activation, leading to large-scale production in an environmentally friendly ways.

It is clear that the material (CLP+KOH-800) contains low amount of sp^2 carbon confirmed by XRD pattern in Figure 8c. Despite this low degree of graphitization according to the XRD results, XPS results confirm a large content of sp^2 character in π aromatic form. The presence of such sp^2 in π aromatic system could enhance electric conductivity which is desired in applications to supercapacitors.

4.3.2 Electrochemical result interpretation

Since the electrochemical result was clearly shown in chapter 3, this section expresses the further interpreted result from chapter 3. From the Figure 9a, the CVs performing at various scan rates (5 mV s^{-1}, 10 mV $s^{-1,}$ 500 mV s^{-1} and 2 V s^{-1}) show two distinct phenomena at low and high scan rate. The first one at low scan rate (5 and 10 mV.s^{-1}) corresponding to the oxidation process of the material which lead to material corrosion. This reaction probably related to the presence of reactive functional groups or unreacted oxygen radicals[68], [69]. This process is irreversible due to the absence of an observable reduction peak during the discharge cycle. The second current drop at low potential could be related to reversible faradaic reactions[70] which would either involve the ad/desorption of OH^- ions on certain electro-active oxygen groups or hydrogen electro-sorption on the carbon framework[69]. However, more insight into the charging mechanisms would be needed to provide definitive answers.

Then the good gravimetric and volumetric performance derived by CVs in Figure 9b combined with a maximum capacitance of 100 F g^{-1} (or 50 F cm^{-3}) at 5mV s^{-1}, these

features place this material in the range of commercially available supercapacitive carbons in term of energy density.

Since the semicircle at high frequency region in Nyquist plot (Figure 11a) indicated the R_{ct} value from faradaic processes, this resistance could either be related to the electrode-current collector contact resistance or the pseudocapacitive phenomenon. The slight increase of R_{ct} upon cycling indicates that the carbon oxidation does not hinder the electrical contact or the pseudo-capacitive mechanisms.

Furthermore, the shift between resistive and capacitive regime indicate that the electrical double layer is not able to form freely from the electrode surface towards the bulk of the electrolyte since it is confined by the mesoporosity of the electrode (pores up to 50 nm). This phenomenon is observed in most supercapacitive porous carbons. The relaxation time characterizes the shifting frequency characteristic of the material. CLP+KOH-800 is typically in the range of microporous endohedral carbons, which usually exhibit slower relaxation times than porous carbons with exohedral porosity such as certain graphene- or CNT-based architectures, providing them with rapid kinetics (τ_{relax} below 100 ms). However, a slight increase of the relaxation time can be attributed to the oxidation of the pores surface, which might slow down ions movements through the porous structure.

According to the Ragone plot in Figure 15b, the material (CLP+KOH-800) shows commensurate properties compared to the commercial carbon materials in both term of energy density and power density. Thanks to the free-standing electrode configuration, the volumetric performances are enhanced (~2 Wh L^{-1} and ~10 kW L^{-1}) compared to electrodes manufactured by coated carbon paste on metal foils, while keeping the manufacturing process simple and low-toxicity. These are promising results, knowing that the performances of this material can easily be improved by modifying the microporous structure via an improvement of the synthesis process more adapted to this type of bio-resource.

CHAPTER 5

CONCLUSION

Magnetic carbon composite adsorbents and carbon-based supercapacitor electrode with excellent performance were successfully prepared from solid and liquid products, respectively in a sustainable way, from low-temperature HTC of water hyacinth. The as-prepared adsorbent shows superior adsorption efficiency towards representative toxic organic compounds in term of both kinetics and adsorption capacity at the equilibrium and also retained good magnetic properties even after use in adsorption. This is due to the presence of high specific surface area and large mesoporosity of the magnetic carbon composite. Furthermore, the good-performance supercapacitor electrode with extremely high surface area can facilely be prepared with the liquid product by employing relatively low amount of KOH. The liquid-derived carbon electrode had high specific capacitance and good capacitance retention, confirming good electrochemical performance. This work demonstrated a simple way to produce functional carbon materials and the use of both solid and liquid HTC products from embarrassing water hyacinth via a more environmentally friendly method. Developing such high value-added carbon-based materials with zero-waste production can facilitate solutions to environmental and energy issues.

BIBLIOGRAPHY

[1] M. Karthik, E. Redondo, E. Goikolea, V. Roddatis, S. Doppiu, and R. Mysyk, "Effect of Mesopore Ordering in Otherwise Similar Micro/Mesoporous Carbons on the High-Rate Performance of Electric Double-Layer Capacitors," *J. Phys. Chem. C*, vol. 118, no. 48, pp. 27715–27720, Dec. 2014.

[2] V. Guna, M. Ilangovan, M. G. A. Prasad, and N. Reddy, "Water Hyacinth: A Unique Source for Sustainable Materials and Products," *Acs Sustain. Chem. Eng.*, vol. 5, no. 6, pp. 4478–4490, 2017.

[3] T. F. Rakotoarisoa, T. Richter, H. Rakotondramanana, and J. Mantilla-Contreras, "Turning a Problem Into Profit: Using Water Hyacinth (Eichhornia crassipes) for Making Handicrafts at Lake Alaotra, Madagascar," *Econ. Bot.*, vol. 70, no. 4, pp. 365–379, 2016.

[4] R. Sindhu *et al.*, "Water hyacinth a potential source for value addition: An overview," *Bioresour. Technol.*, vol. 230, pp. 152–162, 2017.

[5] K. Wu *et al.*, "Large and porous carbon sheets derived from water hyacinth for high-performance supercapacitors," *RSC Adv.*, vol. 6, no. 36, pp. 29996–30003, 2016.

[6] Y. Ding *et al.*, "Competitive removal of Cd(ii) and Pb(ii) by biochars produced from water hyacinths: performance and mechanism," *RSC Adv.*, vol. 6, no. 7, pp. 5223–5232, 2016.

[7] F. Zhang *et al.*, "Efficiency and mechanisms of Cd removal from aqueous solution by biochar derived from water hyacinth (Eichornia crassipes)," *J. Environ. Manage.*, vol. 153, pp. 68–73, 2015.

[8] K. W. Zheng *et al.*, "The porous carbon derived from water hyacinth with well-designed hierarchical structure for supercapacitors," *J. Power Sources*, vol. 366, pp. 270–277, 2017.

[9] G. Zeng, B. L. Zhou, L. C. Yi, H. Li, X. Hu, and Y. Li, "Green and facile fabrication of hierarchical N-doped porous carbon from water hyacinths for high performance lithium/sodium ion batteries," *Sustain. Energy Fuels*, vol. 2, no. 4, pp. 855–861, 2018.

[10] M. A. Rahman, "Pyrolysis of water hyacinth in a fixed bed reactor: Parametric effects on product distribution, characterization and syngas evolutionary

behavior," *Waste Manag.*, vol. 80, pp. 310–318, 2018.

[11] B. Zhang, Z. P. Zhong, T. Li, Z. Y. Xue, and R. Ruan, "Bio-oil production from sequential two-step microwave-assisted catalytic fast pyrolysis of water hyacinth using Ce-doped gamma-Al2O3/ZrO2 composite mesoporous catalyst," *J. Anal. Appl. Pyrolysis*, vol. 132, pp. 143–150, 2018.

[12] A. Jain, R. Balasubramanian, and M. P. Srinivasan, "Hydrothermal conversion of biomass waste to activated carbon with high porosity: A review," *Chem. Eng. J.*, vol. 283, pp. 789–805, 2016.

[13] M.-M. Titirici, R. J. White, C. Falco, and M. Sevilla, "Black perspectives for a green future: hydrothermal carbons for environment protection and energy storage," *Energy Environ. Sci.*, vol. 5, no. 5, pp. 6796–6822, 2012.

[14] N. Rattanachueskul, A. Saning, S. Kaowphong, N. Chumha, and L. Chuenchom, "Magnetic carbon composites with a hierarchical structure for adsorption of tetracycline, prepared from sugarcane bagasse via hydrothermal carbonization coupled with simple heat treatment process," *Bioresour. Technol.*, vol. 226, pp. 164–172, 2017.

[15] Z. G. Liu, F. S. Zhang, and J. Z. Wu, "Characterization and application of chars produced from pinewood pyrolysis and hydrothermal treatment," *Fuel*, vol. 89, no. 2, pp. 510–514, 2010.

[16] J. Fang, L. Zhan, Y. S. Ok, and B. Gao, "Minireview of potential applications of hydrochar derived from hydrothermal carbonization of biomass," *J. Ind. Eng. Chem.*, vol. 57, pp. 15–21, 2018.

[17] K. Nakason, B. Panyapinyopol, V. Kanokkantapong, N. Viriya-empikul, W. Kraithong, and P. Pavasant, "Hydrothermal carbonization of unwanted biomass materials: Effect of process temperature and retention time on hydrochar and liquid fraction," *J. Energy Inst.*, vol. 91, no. 5, pp. 786–796, 2018.

[18] S. L. Zhou *et al.*, "Covalently linked organo-sulfonic acid modified titanate nanotube hybrid nanostructures for the catalytic esterification of levulinic acid with n-butyl alcohol," *Chem. Eng. J.*, vol. 361, pp. 571–577, 2019.

[19] J. Molleti, M. S. Tiwari, and G. D. Yadav, "Novel synthesis of Ru/OMS catalyst by solvent-free method: Selective hydrogenation of levulinic acid to gamma-valerolactone in aqueous medium and kinetic modelling," *Chem. Eng. J.*, vol.

334, pp. 2488–2499, 2018.

[20] H. Chen, H. H. Ruan, X. L. Lu, J. Fu, T. Langrish, and X. Y. Lu, “Catalytic conversion of furfural to methyl levulinate in a single-step route over Zr/SBA-15 in near-critical methanol,” *Chem. Eng. J.*, vol. 333, pp. 434–442, 2018.

[21] L. F. Zhu, F. Shen, R. L. Smith, L. L. Yan, L. Y. Li, and X. H. Qi, “Black liquor-derived porous carbons from rice straw for high-performance supercapacitors,” *Chem. Eng. J.*, vol. 316, pp. 770–777, 2017.

[22] C. X. Bai, L. F. Zhu, F. Shen, and X. H. Qi, “Black liquor-derived carbonaceous solid acid catalyst for the hydrolysis of pretreated rice straw in ionic liquid,” *Bioresour. Technol.*, vol. 220, pp. 656–660, 2016.

[23] L. C. Cao *et al.*, “Microwave-assisted low-temperature hydrothermal treatment of red seaweed (Gracilaria lemaneiformis) for production of levulinic acid and algae hydrochar,” *Bioresour. Technol.*, vol. 273, pp. 251–258, 2019.

[24] A. Kruse, A. Funke, and M.-M. Titirici, “Hydrothermal conversion of biomass to fuels and energetic materials,” *Curr. Opin. Chem. Biol.*, vol. 17, no. 3, pp. 515–521, 2013.

[25] C. Chiou, “Fundamentals of the Adsorption Theory,” 2003, pp. 39–52.

[26] S. Karimi, M. Tavakkoli Yaraki, and R. R. Karri, “A comprehensive review of the adsorption mechanisms and factors influencing the adsorption process from the perspective of bioethanol dehydration,” *Renew. Sustain. Energy Rev.*, vol. 107, pp. 535–553, 2019.

[27] J.-P. Simonin, “On the comparison of pseudo-first order and pseudo-second order rate laws in the modeling of adsorption kinetics,” *Chem. Eng. J.*, vol. 300, pp. 254–263, 2016.

[28] Y. S. Ho and G. McKay, “Pseudo-second order model for sorption processes,” *Process Biochem.*, vol. 34, no. 5, pp. 451–465, 1999.

[29] R. Kecili and C. M. Hussain, “Chapter 4 - Mechanism of Adsorption on Nanomaterials,” C. M. B. T.-N. in C. Hussain, Ed. Elsevier, 2018, pp. 89–115.

[30] C. Ng, J. N. Losso, W. E. Marshall, and R. M. Rao, “Freundlich adsorption isotherms of agricultural by-product-based powdered activated carbons in a geosmin–water system,” *Bioresour. Technol.*, vol. 85, no. 2, pp. 131–135, 2002.

[31] A. González, E. Goikolea, J. A. Barrena, and R. Mysyk, "Review on supercapacitors: Technologies and materials," *Renew. Sustain. Energy Rev.*, vol. 58, pp. 1189–1206, 2016.

[32] Poonam, K. Sharma, A. Arora, and S. K. Tripathi, "Review of supercapacitors: Materials and devices," *J. Energy Storage*, vol. 21, pp. 801–825, 2019.

[33] B. K. Kim, S. Sy, A. Yu, and J. Zhang, "Electrochemical Supercapacitors for Energy Storage and Conversion," *Handbook of Clean Energy Systems*. pp. 1–25, 16-Jul-2015.

[34] Y. Wang, Y. Song, and Y. Xia, "Electrochemical capacitors: mechanism, materials, systems, characterization and applications," *Chem. Soc. Rev.*, vol. 45, no. 21, pp. 5925–5950, 2016.

[35] N. F. Ghadikolaei, E. Kowsari, S. Balou, A. Moradi, and F. A. Taromi, "Preparation of porous biomass-derived hydrothermal carbon modified with terminal amino hyperbranched polymer for prominent Cr(VI) removal from water," *Bioresour. Technol.*, vol. 288, p. 121545, 2019.

[36] Y. Li *et al.*, "Hydrochars from bamboo sawdust through acid assisted and two-stage hydrothermal carbonization for removal of two organics from aqueous solution," *Bioresour. Technol.*, vol. 261, pp. 257–264, 2018.

[37] J. Ifthikar *et al.*, "Highly Efficient Lead Distribution by Magnetic Sewage Sludge Biochar: Sorption Mechanisms and Bench Applications," *Bioresour. Technol.*, vol. 238, pp. 399–406, 2017.

[38] W. Astuti, T. Sulistyaningsih, E. Kusumastuti, G. Yanny Ratna Sari Thomas, and R. Yogaswara Kusnadi, *Thermal conversion of pineapple crown leaf waste to magnetized activated carbon for dye removal*, vol. 287. 2019.

[39] Y. Han, X. Cao, X. Ouyang, S. Sohi, and J. Chen, *Adsorption kinetics of magnetic biochar derived from peanut hull on removal of Cr (VI) from aqueous solution: Effects of production conditions and particle size*, vol. 145. 2016.

[40] Y. An *et al.*, *Synthesis of Hierarchically Porous Nitrogen-Doped Carbon Nanosheets from Agaric for High-Performance Symmetric Supercapacitors*, vol. 4. 2017.

[41] X. Song, X. Ma, Y. Li, L. Ding, and R. Jiang, "Tea waste derived microporous

active carbon with enhanced double-layer supercapacitor behaviors," *Appl. Surf. Sci.*, vol. 487, pp. 189–197, 2019.

[42] E. Elaiyappillai *et al.*, "Low cost activated carbon derived from Cucumis melo fruit peel for electrochemical supercapacitor application," *Appl. Surf. Sci.*, vol. 486, pp. 527–538, 2019.

[43] M. Sevilla and A. B. Fuertes, "A Green Approach to High-Performance Supercapacitor Electrodes: The Chemical Activation of Hydrochar with Potassium Bicarbonate," *ChemSusChem*, vol. 9, no. 14, pp. 1880–1888, Jul. 2016.

[44] G. A. Ferrero, A. B. Fuertes, and M. Sevilla, "From Soybean residue to advanced supercapacitors," *Sci. Rep.*, vol. 5, p. 16618, Nov. 2015.

[45] V. Fierro, V. Torné-Fernández, and A. Celzard, "Methodical study of the chemical activation of Kraft lignin with KOH and NaOH," *Microporous Mesoporous Mater.*, vol. 101, no. 3, pp. 419–431, 2007.

[46] G. A. Ferrero, A. B. Fuertes, and M. Sevilla, "N-doped porous carbon capsules with tunable porosity for high-performance supercapacitors," *J. Mater. Chem. A*, vol. 3, no. 6, pp. 2914–2923, 2015.

[47] Z. Daud, M. Z. M. Hatta, A. S. M. Kassim, H. Awang, and A. M. Aripin, "Exploring of Agro Waste (Pineapple Leaf, Corn Stalk, and Napier Grass) by Chemical Composition and Morphological Study," *Bioresources*, vol. 9, no. 1, pp. 872–880, 2014.

[48] K. R. Arturi *et al.*, "Molecular footprint of co-solvents in hydrothermal liquefaction (HTL) of Fallopia Japonica," *J. Supercrit. Fluids*, vol. 143, pp. 211–222, 2019.

[49] S. Jadsadajerm, T. Muangthong-on, J. Wannapeera, H. Ohgaki, K. Miura, and N. Worasuwannarak, "Degradative solvent extraction of biomass using petroleum based solvents," *Bioresour. Technol.*, vol. 260, pp. 169–176, 2018.

[50] Y. L. Hu, L. Y. Qi, S. H. Feng, A. Bassi, and C. Xu, "Comparative studies on liquefaction of low-lipid microalgae into bio-crude oil using varying reaction media," *Fuel*, vol. 238, pp. 240–247, 2019.

[51] A. Jedrzak, T. Rebis, M. Nowicki, K. Synoradzki, R. Mrowczynski, and T.

Jesionowski, “Polydopamine grafted on an advanced Fe3O4/lignin hybrid material and its evaluation in biosensing,” *Appl. Surf. Sci.*, vol. 455, pp. 455–464, 2018.

[52] Y. Park and J. S. Lee, “Flexible Multistate Data Storage Devices Fabricated Using Natural Lignin at Room Temperature,” *ACS Appl. Mater. Interfaces*, vol. 9, no. 7, pp. 6207–6212, 2017.

[53] J. D. Dai *et al.*, “Fe3C/Fe/C Magnetic Hierarchical Porous Carbon with Micromesopores for Highly Efficient Chloramphenicol Adsorption: Magnetization, Graphitization, and Adsorption Properties Investigation,” *Ind. Eng. Chem. Res.*, vol. 57, no. 10, pp. 3510–3522, 2018.

[54] W. B. Wang, H. X. Zhang, J. F. Shen, and M. X. Ye, “Facile preparation of magnetic chitosan/poly (vinyl alcohol) hydrogel beads with excellent adsorption ability via freezing-thawing method,” *Colloids Surfaces a-Physicochemical Eng. Asp.*, vol. 553, pp. 672–680, 2018.

[55] R. A. L. Sobrinho, G. R. S. Andrade, L. P. Costa, M. J. B. de Souza, A. de Souza, and I. F. Gimenez, “Ordered micro-mesoporous carbon from palm oil cooking waste via nanocasting in HZSM-5/SBA-15 composite: Preparation and adsorption studies,” *J. Hazard. Mater.*, vol. 362, pp. 53–61, 2019.

[56] X. Zhu, Y. Liu, G. Luo, F. Qian, S. Zhang, and J. Chen, “Facile Fabrication of Magnetic Carbon Composites from Hydrochar via Simultaneous Activation and Magnetization for Triclosan Adsorption,” *Environ. Sci. Technol.*, vol. 48, no. 10, pp. 5840–5848, May 2014.

[57] X. D. Zhu *et al.*, “Controllable synthesis of magnetic carbon composites with high porosity and strong acid resistance from hydrochar for efficient removal of organic pollutants: An overlooked influence,” *Carbon N. Y.*, vol. 99, pp. 338–347, 2016.

[58] M. J. Ahmed, P. U. Okoye, E. H. Hummadi, and B. H. Hameed, “High-performance porous biochar from the pyrolysis of natural and renewable seaweed (Gelidiella acerosa) and its application for the adsorption of methylene blue,” *Bioresour. Technol.*, vol. 278, pp. 159–164, 2019.

[59] F. F. Ma, D. Zhang, T. Huang, N. Zhang, and Y. Wang, “Ultrasonication-assisted deposition of graphene oxide on electrospun poly (vinylidene fluoride)

membrane and the adsorption behavior," *Chem. Eng. J.*, vol. 358, pp. 1065–1073, 2019.

[60] E. Petala *et al.*, "Nanoscale zero-valent iron supported on mesoporous silica: Characterization and reactivity for Cr(VI) removal from aqueous solution," *J. Hazard. Mater.*, vol. 261, pp. 295–306, 2013.

[61] M. Ruthiraan, E. C. Abdullah, N. M. Mubarak, and M. N. Noraini, "A promising route of magnetic based materials for removal of cadmium and methylene blue from waste water," *J. Environ. Chem. Eng.*, vol. 5, no. 2, pp. 1447–1455, 2017.

[62] H. Ma, J. B. Li, W. W. Liu, M. Miao, B. J. Cheng, and S. W. Zhu, "Novel synthesis of a versatile magnetic adsorbent derived from corncob for dye removal," *Bioresour. Technol.*, vol. 190, pp. 13–20, 2015.

[63] S. Z. Guo, H. C. Xu, F. Zhang, X. X. Zhu, and X. L. Li, "Preparation and adsorption properties of nano magnetite silica gel for methylene blue from aqueous solution," *Colloids Surfaces a-Physicochemical Eng. Asp.*, vol. 546, pp. 244–253, 2018.

[64] B. W. Yu *et al.*, "Magnetic graphene sponge for the removal of methylene blue," *Appl. Surf. Sci.*, vol. 351, pp. 765–771, 2015.

[65] X. G. Huang, X. Z. Zhan, C. L. Wen, F. Xu, and L. J. Luo, "Amino-functionalized magnetic bacterial cellulose/activated carbon composite for Pb2+ and methyl orange sorption from aqueous solution," *J. Mater. Sci. Technol.*, vol. 34, no. 5, pp. 855–863, 2018.

[66] W. L. Shi *et al.*, "Carbon dots decorated magnetic ZnFe2O4 nanoparticles with enhanced adsorption capacity for the removal of dye from aqueous solution," *Appl. Surf. Sci.*, vol. 433, pp. 790–797, 2018.

[67] S. P. Zhang, Y. Y. Dong, Z. Yang, W. B. Yang, J. Q. Wu, and C. Dong, "Adsorption of pharmaceuticals on chitosan-based magnetic composite particles with core-brush topology," *Chem. Eng. J.*, vol. 304, pp. 325–334, 2016.

[68] M. He, K. Fic, E. Frąckowiak, P. Novák, and E. J. Berg, "Ageing phenomena in high-voltage aqueous supercapacitors investigated by in situ gas analysis," *Energy Environ. Sci.*, vol. 9, no. 2, pp. 623–633, 2016.

[69] F. Beguin and E. Frackowiak, *Carbons for Electrochemical Energy Storage and Conversion Systems*, 1st ed. CRC Press, 2009.

[70] Z. Li *et al.*, "Reduced CoNi2S4 nanosheets with enhanced conductivity for high-performance supercapacitors," *Electrochim. Acta*, vol. 278, pp. 33–41, 2018.

VITAE

Name Miss Amonrada Saning

Student ID 5910220075

Educational Attainment

Degree	Name of Institution	Year of Graduation
Bachelor of Science (Chemistry)	Prince of Songkla University	2015

Scholarship Awards during Enrolment

Science Achievement Scholarship of Thailand (SAST)

List of Publication and Proceeding

Rattanachueskul, N., Saning, A., Kaowphong, S., Chumha, N., Chuenchom, L. 2017. Magnetic carbon composites with a hierarchical structure for adsorption of tetracycline, prepared from sugarcane bagasse via hydrothermal carbonization coupled with simple heat treatment process. Bioresour. Technol., 2017, 226, 164–172.

List of Presentation

Saning, A., Ieosakulrat, C., Pakawatpanurut, P., Chuenchom, L. 2018. The application of solid and liquid products from green hydrothermal carbonization of water hyacinth (*Eichhornia crassipes*) used as adsorbent and supercapacitor, PERCH-CIC Congress X: 2018 International Congress for Innovation in Chemistry.